Neutron transport methods for accelerator-driven systems
Grant: DE-PS07-01ID13695
Final Report

Submitted by: Dr. Nicholas Tsoulfanidis, PI, and
Dr. Elmer Lewis, Co-PI

The objective of this project has been to develop computational methods that will enable more effective analysis of Accelerator Driven Systems (ADS). The work is centered at the University of Missouri at Rolla, with a subcontract at Northwestern University, and close cooperation with the Nuclear Engineering Division at Argonne National Laboratory. The work has fallen into three categories. First, the treatment of the source for neutrons originating from the spallation target which drives the neutronics calculations of the ADS. This work was done at the University of Missouri, and carried out primarily by J. Ferrero, a MS NE student and N. Tsoulfanidis . Second, the generalization of the nodal variational method to treat the R-Z geometry configurations frequently needed for scoping calculations in Accelerator Driven Systems. This work was performed primarily by H. Zhang and E. E. Lewis at Northwestern University. Third, the treatment of void regions within variational nodal methods as needed to treat the accelerator beam tube. This work was centered at Argonne National Laboratory in close collaboration with M. A. Smith (a former NEER- supported student) of the Argonne Staff. The eventual aim of all three tasks has been to develop a computational tool based on the Variational Nodal code VARIANT at Argonne National Laboratory suitable for the analysis of accelerator driven systems.

For the first task, a Monte Carlo model of an Accelerator Driven System (ADS) has been developed using the MCNPx code. Our MCNPx model consists of the following major components. (see also our June 2003 report)

1. The proton accelerator tube (Fig. 1, see, App. A)
2. The target
3. Six nuclear fuel assemblies placed symmetrically around the accelerator tube in a cylindrical geometry.(Fig.2, see, App. A)
4. A "blanket" placed between the assemblies and at the periphery of the ADS

Three different models have been developed representing three levels of homogenization . Model 1: Individually modeled fuel rods in each assembly. (Fig. 2) Model 2: Homogenized fuel assemblies in water. Model 3: Homogenized rings of water and water plus nuclear fuel. Neutron fluxes have been computed for the three models and comparisons made. In addition, the neutron fluxes were computed for the three models with and without transuranics (TRU) in the fuel.

The results of the calculations have been presented at the ANS meeting in November 2003 (Ferrero-Tsoulfanidis, 2003) and also incorporated in the M.S. Thesis of Jamie Ferrero at the University of Missouri-Rolla.

The second task, the generalization of the VARIANT code to treat R-Z geometry has been completed. The work through the winter of 2004 is summarized in a paper given at the 2004 PHYSOR conference in Chicago [Zhang & Lewis, 2004A] and is included as Appendix B. A final outcome of the work is given in a paper being submitted to Nuclear Science and Engineering [Zhang and Lewis, 2004B], and it is included as Appendix C.
Two theoretical challenges, which are not present in Cartesian or hexagonal versions of the variational nodal method, are encountered in R-Z geometry. First, there is an angular derivative in the gradient term, and this more closely couples the spatial and angular approximations. Second, the necessity of meeting the correct angular symmetry conditions along the domain centerline requires the introduction of coupled constraints on the spatial and angular trial functions. As a practical matter, the most time-consuming difficulties were encountered in merging the R-Z into the VARIANT code, a code containing well over 100,000 lines of FORTRAN. In addition to the journal article based on this work, a detailed description of the modification and overrides made to the standard VARIANT code is being provided to the staff at Argonne National Laboratory so that the R-Z generalization can become part of their standard code package.

The third task, that of finding an effective method for forming response matrices which are both compatible with VARIANT and capable of treating void regions has been carried out in close collaboration with M. A. Smith and other staff members at Argonne National Laboratory. Treatment of void regions using the even-parity based VARIANT is indeed a challenge, since the basic second-order equations contains the total cross section in the denominator. Some success has been achieved melding the first order form of spherical harmonics equations with VARIANT. This has been reported at the 2004 PHYSOR conference in Chicago [Smith, et. al, 2004] and is included as Appendix D. Recently, a more in depth analysis of various first-order possibilities has been undertaken and reported [Lewis, 2004] and an improved treatment of voids proposed. This work is included as Appendix E. Thus far only X-Y geometry has been treated with success. However, extension to R-Z geometry , once X-Y geometry is mastered appears to be less of a challenge.

In conclusion, major advances have been made in all three aspects of the research, and resulted in published results. Further work, however, is needed to bring together the progress made in advanced algorithms for the treatment of Accelerator Driven Systems.

References

Ferrero J. and Tsoulfanidis N. , ANS Trans. V. 89, p. 635-637, 2003.

Lewis, E. E. (2004), "Much Ado about Nothing: Response Matrices for Void Regions,"
Ann. Nucl. Energy, to appear, Nov. 2004 issue

Smith, M. A., Palmiotti, G., and Lewis, E. E.,(2004), "First-Order Spherical Harmonics Formulation Capable of Treating Low Density and Void Regions within the Framework of VARIANT," Proc. PHYSOR_2004 *Tpg. Mtg on the Physics of Fuel Cycles and Advanced Nuclear Systems: Global Developments*, Chicago, April 2004

Zhang, Hui and Lewis, E. E. (2004A), "The Variational Nodal Method in *R-Z* Geometry," Proc. PHYSOR_2004 *Tpg. Mtg on the Physics of Fuel Cycles and Advanced Nuclear Systems: Global Developments*, Chicago, April 2004

Zhang, Hui and Lewis, E. E. (2004B) "Generalization of the Variational Nodal Method
to Spherical Harmonics Approximations in R-Z Geometry", submitted to *Nucl. Sci. Eng.*

Appendix A

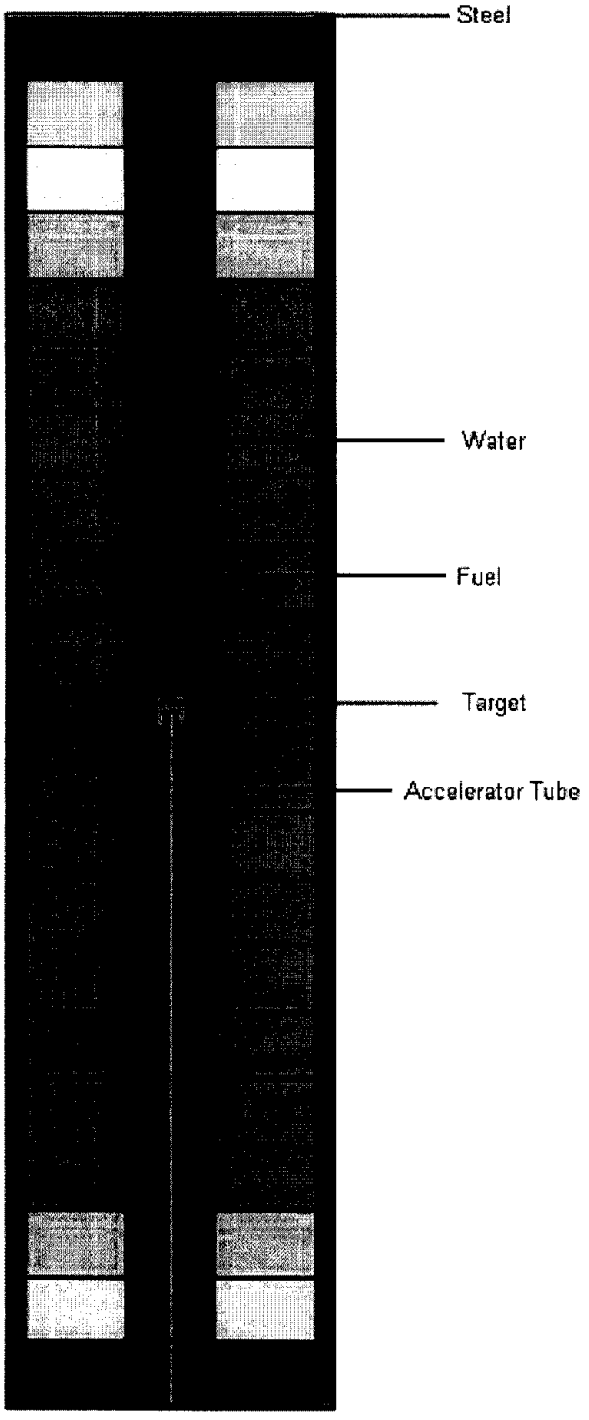

Figure 1. x-z view of homogenized assemblies model

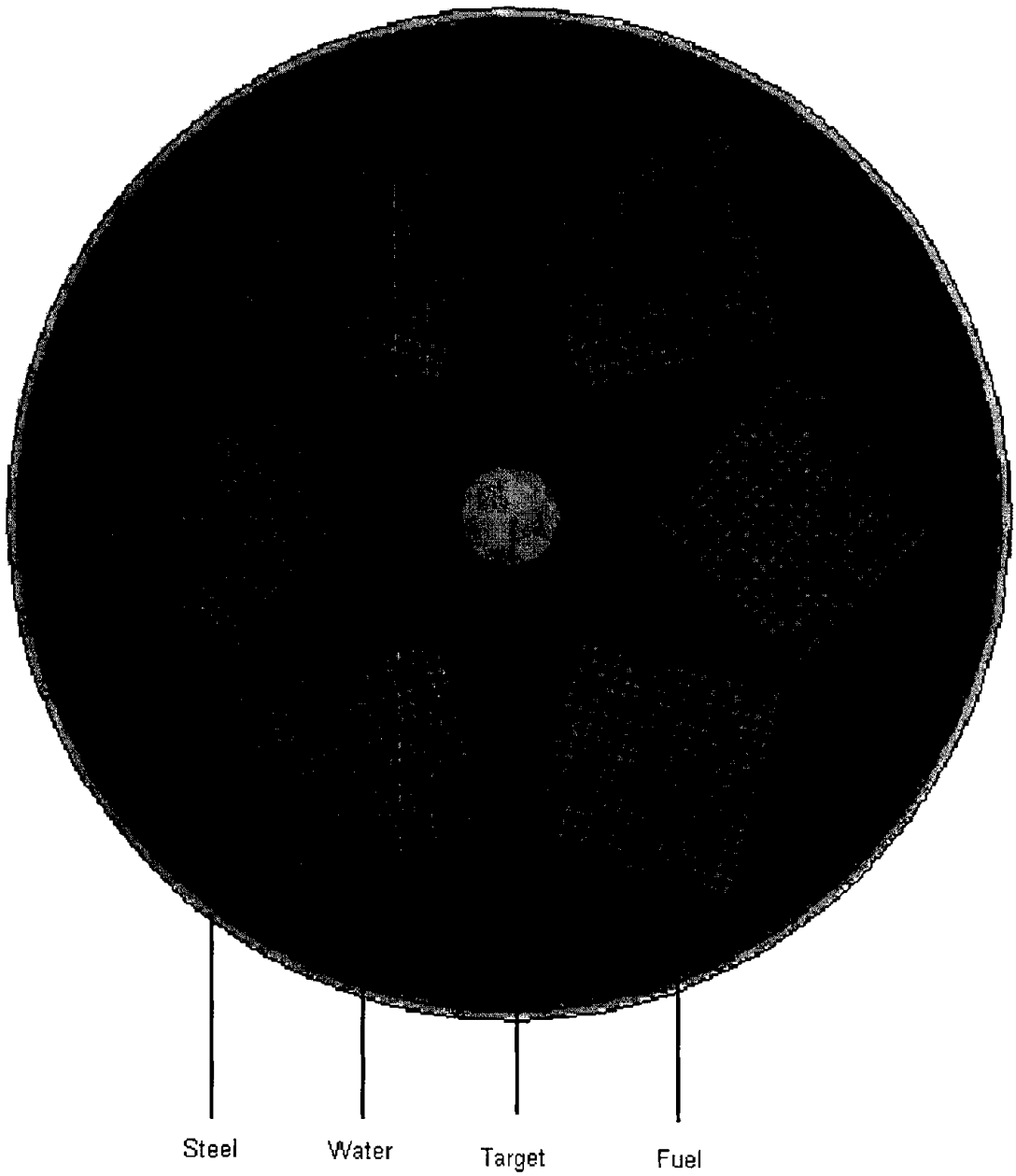

Firgure 2. x-y view of detailed model with rods present in assemblies

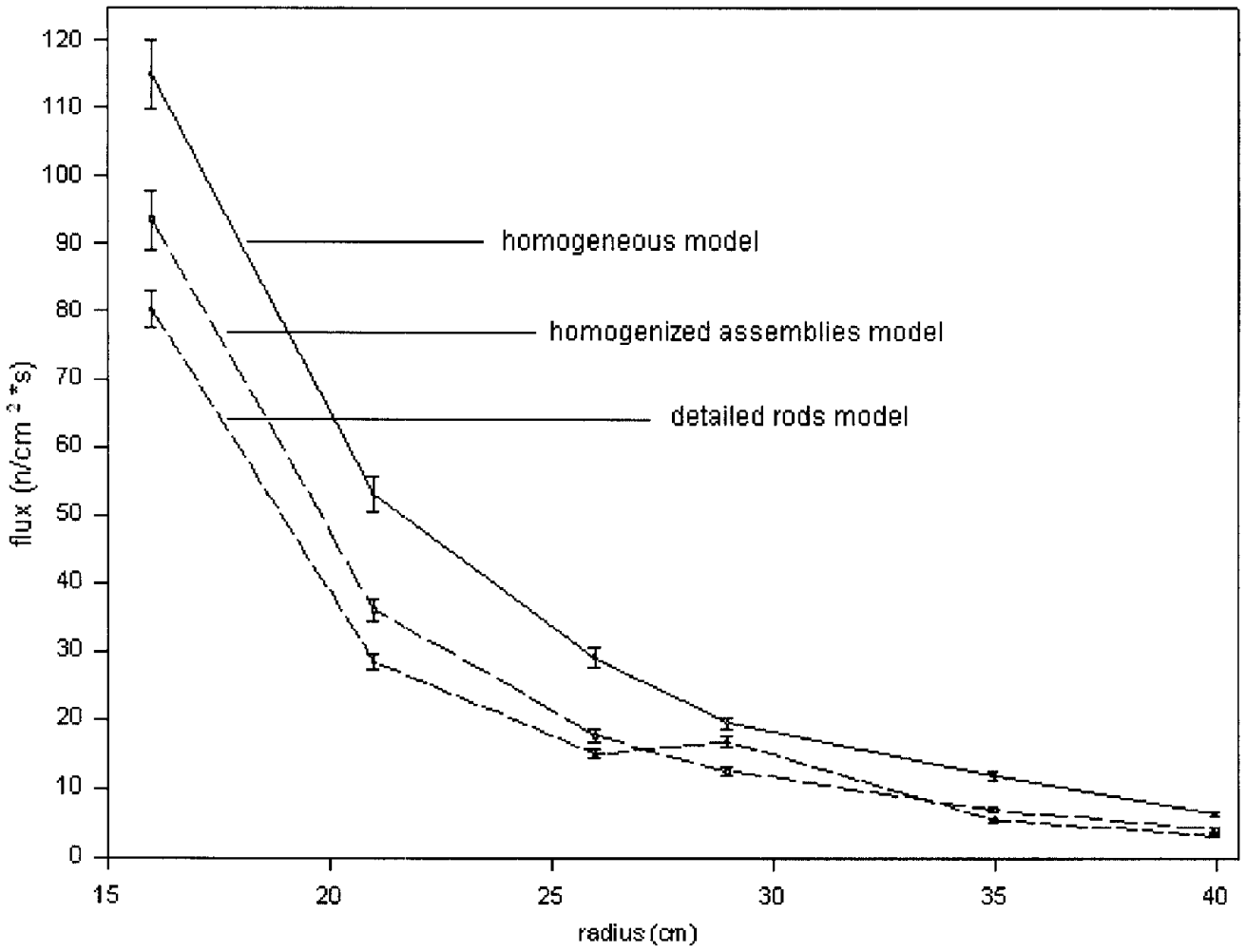

Figure 3. ϕ(relative values) vs. r for all three models; ♦ homogeneous, □ assembly, Δ rods

PHYSOR 2004-The Physics of Fuel Cycles and Advanced Nuclear Systems: Global Developments
Chicago, Illinois, April 25-29, 2004, on CD-ROM, American Nuclear Society, Lagrange Park, IL. (2004)

The Variational Nodal Method in *R-Z* Geometry

Hui Zhang & E. E. Lewis*
Northwestern University, Department of Mechanical Engineering, Evanston, IL 60208 USA

The variational nodal method contained in the Argonne National Laboratory code VARIANT is generalized to include *R-Z* geometry. Spherical harmonic trial functions are used in angle, and polynomials in space. The nodal volumes correspond to toroids, with rectangular cross sections, except along centerline where they are cylinders. The *R-Z* response matrix equations are solved using the iterative methods already contained in VARIANT. Results are given for both a one-group fixed source and a two-group eigenvalue problem.

KEYWORDS: Boltzmann Equation, R-Z Geometry, Neutron Transport, Nodal Method, Spherical Harmonics, Variational Method

1. Introduction

The variational nodal method has found substantial use in both diffusion theory and higher-order spherical harmonics approximations. It has been available in both two- and three-dimensional Cartesian and hexagonal geometries. However, the need sometimes arises for two-dimensional *R-Z* geometry calculations, particularly for scoping studies. The purpose of this work is to develop an *R-Z* option for the Argonne National Laboratory variational nodal code VARIANT [1, 2].

2. Theory

2.1 Variational Formulation

The variational nodal method is a primal hybrid finite element representation of the even-parity form of the transport equation. In the hybrid formulation, the problem domain V is decomposed into subdomains V_v (also called elements or nodes):

$$V = \sum_v V_v . \tag{1}$$

Within each node, the even-parity form of the transport equation is solved in space ($\vec{r}$) and angle ($\hat{\Omega}$):

$$-\hat{\Omega}\cdot\vec{\nabla}\sigma^{-1}\hat{\Omega}\cdot\vec{\nabla}\psi^{+}(\vec{r},\hat{\Omega})+\sigma\ \psi^{+}(\vec{r},\hat{\Omega})=\sigma_s\int d\hat{\Omega}'\psi^{+}(\vec{r},\hat{\Omega}')+s(\vec{r}),\quad \vec{r}\in V_v \tag{2}$$

where ψ^{+} is the even parity flux component, σ and σ_s the total and scattering cross sections and s the group source. The odd-parity flux ψ^{-}, which is related to ψ^{+} by

* Corresponding author, Tel. 847-491-3579, FAX 847-491-3915, E-mail: e-lewis@northwestern.edu

$$\hat{\Omega}\cdot\vec{\nabla}\psi^{+}(\vec{r},\hat{\Omega})+\sigma\psi^{-}(\vec{r},\hat{\Omega})=0, \qquad \vec{r}\in\Gamma_{\nu} \tag{3}$$

is defined only along the node interface Γ_{ν} as a Lagrange multiplier.

The functional for the variational nodal method is given as a superposition of nodal contributions:

$$F[\psi^{+},\psi^{-}]=\sum_{\nu}F_{\nu}[\psi^{+},\psi^{-}], \tag{4}$$

where

$$F_{\nu}[\psi^{+},\psi^{-}]=\int_{\nu}dV\left\{\int d\Omega[\sigma^{-1}(\hat{\Omega}\cdot\vec{\nabla}\psi^{+})^{2}+\sigma\psi^{+^{2}}]-\sigma_{s}\phi^{2}-2\phi s\right\}+2\int_{\nu}d\Gamma\int d\Omega\hat{\Omega}\cdot\hat{n}\psi^{+}\psi^{-}, \tag{5}$$

and ϕ is the scalar flux. This functional must be stationary with respect to arbitrary variations $\tilde{\psi}^{+}$ and $\tilde{\psi}^{-}$ about the true solutions $\psi^{+}$and ψ^{-}. Thus, we make the replacements $\psi^{+}\rightarrow\psi^{+}+\delta\tilde{\psi}^{+}$ and $\psi^{-}\rightarrow\psi^{-}+\varepsilon\tilde{\psi}^{-}$ where δ and ε are small positive constants, and require the linear terms in δ and ε to vanish. Setting the linear term in δ to zero yields the weak form of Eq. (2):

$$\int_{\nu}dV\int d\Omega[\sigma^{-1}(\hat{\Omega}\cdot\vec{\nabla}\tilde{\psi}^{+})(\hat{\Omega}\cdot\vec{\nabla}\psi^{+})+\tilde{\psi}^{+}(\sigma\psi^{+}-\sigma_{s}\phi-s)]+\int_{\nu}d\Gamma\int d\Omega\hat{\Omega}\cdot\hat{n}\tilde{\psi}^{+}\psi^{-}=0, \tag{6}$$

and applying the divergence theorem yields

$$\int_{\nu}dV\int d\Omega\tilde{\psi}^{+}(-\hat{\Omega}\cdot\vec{\nabla}\sigma^{-1}\hat{\Omega}\cdot\vec{\nabla}\psi^{+}+\sigma\psi^{+}-\sigma_{s}\phi-s)+\int_{\nu}d\Gamma\int d\Omega\hat{\Omega}\cdot\hat{n}\tilde{\psi}^{+}(\psi^{-}+\sigma^{-1}\hat{\Omega}\cdot\vec{\nabla}\psi^{+})=0. \tag{7}$$

Clearly, Eq. (2) must be satisfied if the volume integral is to vanish for arbitrary $\tilde{\psi}^{+}$, and Eq. (3) must be met at the interface for the surface integral to vanish. The continuity conditions across nodal interfaces may be stated as follows. Since the Lagrange multiplier ψ^{-} and its variation $\tilde{\psi}^{-}$ are uniquely defined at the interface, two conditions are imposed. First, the surface integral in Eq. (7) imposes continuity on $\sigma^{-1}\hat{\Omega}\cdot\vec{\nabla}\psi^{+}$. Second, requiring the linear term in ε to vanish yields for each nodal interface, say between nodes V_{ν} and $V_{\nu'}$, a condition of the form

$$\int_{\nu}d\Gamma\int d\Omega\hat{\Omega}\cdot\hat{n}\tilde{\psi}^{-}(\psi^{+}-\psi'^{+})=0, \tag{8}$$

since $\hat{n}_{\nu}=-\hat{n}_{\nu'}$. Thus ψ^{+} must be continuous across the interface.

2.2. Cylindrical Coordinates (r, z)

The *R-Z* cylindrical coordinates system is shown in Figure 1, together with an angular-direction coordinates system used to define the particle direction $\hat{\Omega}$. In this system, a spatial point is defined by its (r, z) coordinate and

$$\hat{\Omega}=\Omega_r\hat{r}+\Omega_\omega\hat{\omega}+\Omega_z\hat{z}, \tag{9}$$

where

$$\begin{aligned}\Omega_r &=(1-\mu^2)^{1/2}\cos\omega,\\ \Omega_\omega &=(1-\mu^2)^{1/2}\sin\omega,\\ \Omega_z &=\mu\end{aligned} \tag{10}$$

with $\mu=\cos\theta$. The $\hat{\Omega}\cdot\vec{\nabla}$ may be determined by [3, 4]

$$\hat{\Omega}\cdot\vec{\nabla}=\Omega_r\frac{\partial}{\partial r}-\frac{1}{r}\Omega_\omega\frac{\partial}{\partial\omega}+\Omega_z\frac{\partial}{\partial z}, \tag{11}$$

and the incremental angle is defined as $d\Omega=(4\pi)^{-1}d\mu d\omega$.

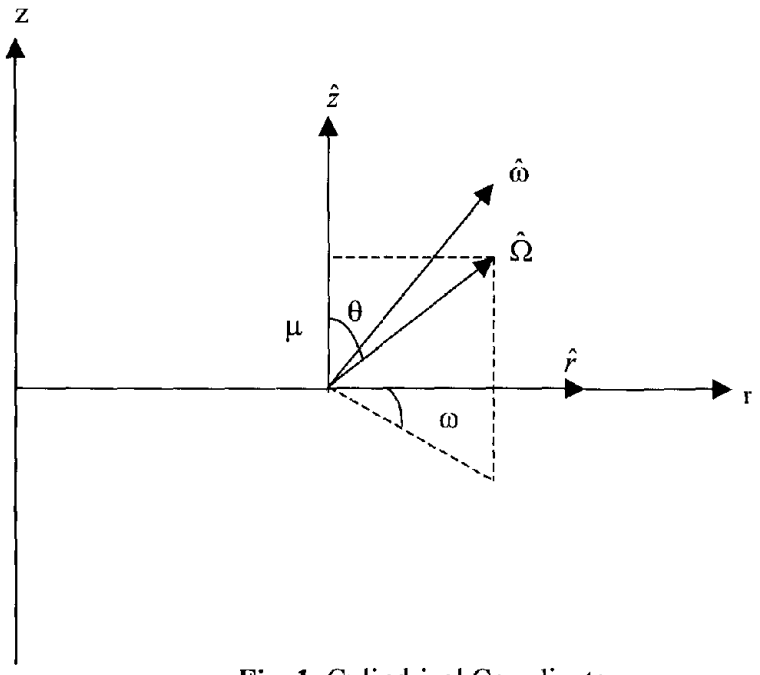

Fig. 1 Cylindrical Coordinates

2.3. Discretization

We begin by considering a rectangular node in r, z bounded on left and right by $r_l\le r\le r_r$ and on bottom and top by $z_b\le z\le z_t$ as shown in Figure 2. We expand the even-parity flux coefficients within the node as

$$\psi^+(r,z,\hat{\Omega})=\mathbf{g}^T(\hat{\Omega})\otimes\mathbf{f}^T(r,z)\xi_v. \qquad r_l\le r\le r_r, z_b\le z\le z_t \tag{12}$$

Here $\otimes$ denotes the Kronecker product, and $\mathbf{g}(\hat{\Omega})$ is vector of even-order spherical harmonics with M terms obey the orthonormal condition

$$\int d\hat{\Omega}\mathbf{g}(\hat{\Omega})\mathbf{g}^T(\hat{\Omega}) = \mathbf{I}_M . \tag{13}$$

The spatial trial functions $\mathbf{f}(r,z)$ are complete polynomials. They are Legendre polynomials in z and also constructed to be orthogonal in r, so that

$$\frac{1}{V_v}\int_v dV\mathbf{f}(r,z)\mathbf{f}^T(r,z) = \mathbf{I}_l , \tag{14}$$

In R-Z geometry, $V_v = 2\pi(r_r^2 - r_l^2)(z_t - z_b)$ and

$$\int_v dV(\cdot) = 2\pi\int_{r_l}^{r_r} dr\, r\int_{z_b}^{z_t} dz(\cdot) \tag{15}$$

The vector ξ_v in Eq, (12) contains the unknown coefficients.

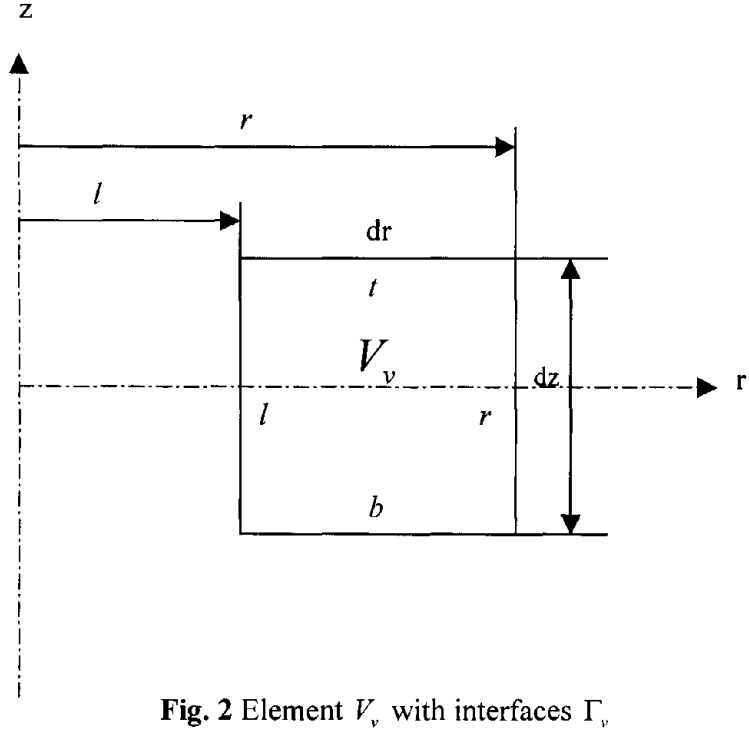

Fig. 2 Element V_v with interfaces Γ_v

Along the node interfaces, we make the expansions

$$\psi^-(\vec{r},\hat{\Omega}) = \mathbf{k}_\gamma^T(\hat{\Omega}) \otimes h_\gamma^T(z)\chi_\gamma^-, \qquad \vec{r} \in \Gamma_r, \Gamma_l$$

and (16)

$$\psi^-(\vec{r},\hat{\Omega}) = \mathbf{k}_\gamma^T(\hat{\Omega}) \otimes h_\gamma^T(z)\chi_\gamma^-, \qquad \vec{r} \in \Gamma_t, \Gamma_b$$

where $\mathbf{k}_\gamma(\hat{\Omega})$ is vector of odd-order spherical harmonics in which the angular coordinates have been rotated such that the polar angle, $\mu = \hat{\Omega} \cdot \hat{n}_\gamma$, is taken with respect to the surface normal. They obey the orthonormal conditions

$$\int d\Omega \mathbf{k}_\gamma(\hat{\Omega})\mathbf{k}_\gamma^T(\hat{\Omega}) = \mathbf{I}_N$$

and $\gamma = r,t,l,b$ (17)

$$\int d\Omega \mathbf{g}(\hat{\Omega})\mathbf{k}_\gamma^T(\hat{\Omega}) = \mathbf{0}$$

The spatial trial functions $\mathbf{h}_\gamma$ are set sets of orthogonal polynomials defined along the interfaces.

The source and the scalar flux may be approximated as

$$\mathbf{s} = \mathbf{w}s(r,z) \tag{18}$$

and $r_l \le r \le r_r, z_b \le z \le z_t$

$$\phi(\vec{r}) = \mathbf{w}^T \otimes \mathbf{f}^T(r,z)\xi_\nu \tag{19}$$

with $[\mathbf{w}]_m = \delta_{m1}$.

The nodal volumes corresponding to the response matrices will be toroids with rectangular cross sections in the r, z plane. The central nodes, however, are cylinders with three surfaces. The centerline symmetry condition that

$$\lim_{r\to\infty} \psi^\pm(\vec{r},\hat{\Omega}) = \psi^\pm(z,\theta) \tag{20}$$

requires that the central nodes contain two sets of trial functions for ψ^+ and for ψ^- when spherical harmonics are employed. Only even functions in r are included in the spatial trial function sets for the Y_{l0} terms, which are independent of ω, causing the radial derivative vanishes at $r = 0$; only odd functions of r are included for the ω dependent Y_{lm}, $m \neq 0$ terms, causing them to vanish at the origin. With these stipulations, the singularities that would otherwise be encountered in applying the operator of Eq. (11) are removed. Note, also, that unlike Cartesian geometry, each response matrix in the radial direction is unique, even though the cross sections and the widths and heights of the nodes are same.

2.4. Response Matrix Evaluation

Response matrices are obtained from the foregoing space-angle trial functions by inserting them into Eqs. (4) and (5). This reduces the functional to the algebraic form:

$$F = \sum_{\nu} F_{\nu}[\zeta_{\nu}, \chi_{\nu}] \tag{21}$$

and

$$F_{\nu}[\zeta_{\nu}, \chi_{\nu}] = \zeta_{\nu}^{T} \mathbf{A}_{\nu} \zeta_{\nu} - 2\zeta_{\nu}^{T} \mathbf{s}_{\nu} + 2\zeta_{\nu}^{T} \mathbf{M}_{\nu} \chi_{\nu}. \tag{22}$$

The matrix $\mathbf{A}_{\mathrm{V}}$ is given as

$$\mathbf{A}_{\nu} = \sigma_{\nu}^{-1} \mathbf{H}_{kk'} \otimes \int_{\nu} dV (\nabla_k \mathbf{f})(\nabla_{k'} \mathbf{f}^{T}) + (\sigma_{\nu} \mathbf{I}_{M} - \sigma_{s\nu} \mathbf{w}\mathbf{w}^{T}) \otimes V_{\nu} \mathbf{I}_{l}, \tag{23}$$

where repeated subscripts k or k' indicates summation with $k, k' = r, \omega, z$, and

$$\begin{aligned} \nabla_r \mathbf{f} &= \partial \mathbf{f} / \partial r, \\ \nabla_{\omega} \mathbf{f} &= \mathbf{f} / r, \\ \nabla_z \mathbf{f} &= \partial \mathbf{f} / \partial z. \end{aligned} \tag{24}$$

The incremental spatial volume is given by $dV = 2\pi r dr dz$.

Each of the elements of $\mathbf{A}_{\mathrm{V}}$ is given in terms of integrals over known spatial or angular trial functions:

$$\mathbf{H}_{kk'} = \int d\Omega \Omega_k \Omega_{k'} \breve{\mathbf{g}}_k \breve{\mathbf{g}}_{k'}^{T}, \tag{25}$$

where

$$\begin{aligned} \breve{\mathbf{g}}_{r,z} &= \mathbf{g}, \\ \breve{\mathbf{g}}_{\omega} &= -\partial \mathbf{g} / \partial \omega. \end{aligned} \tag{26}$$

The source is

$$\mathbf{s}_{\nu} = \int_{\nu} dV \mathbf{s} \otimes \mathbf{f}. \tag{27}$$

The surface coefficients are partitioned according to the four interfaces:

$$\chi_{\nu} = \begin{bmatrix} \chi_r' \\ \chi_t' \\ \chi_l' \\ \chi_b' \end{bmatrix} \tag{28}$$

The $\mathbf{M}_{\mathrm{v}}$ matrix is then given as

$$\mathbf{M}_{\nu} = [\mathbf{M}_r', \mathbf{M}_t', \mathbf{M}_l', \mathbf{M}_b'], \tag{29}$$

$$\mathbf{M}_{\gamma}' = \mathbf{E}_{\gamma} \otimes \mathbf{D}_{\gamma}, \qquad \gamma = r, t, l, b \tag{30}$$

where

$$\vec{\mathbf{E}}_{\gamma} = \int d\Omega \hat{\Omega} \cdot \hat{n}_{\gamma} \mathbf{g}(\hat{\Omega}) \mathbf{k}_{\gamma}^{T}(\hat{\Omega}), \tag{31}$$

and

$$\mathbf{D}_\gamma = 2\pi r_\gamma \int_{z_b}^{z_t} dz \mathbf{f}(r_\gamma, z)\mathbf{h}_\gamma^T(z), \qquad \gamma = r,l$$
$$\mathbf{D}_\gamma = 2\pi \int_{r_l}^{r_r} dr r \mathbf{f}(r, z_\gamma)\mathbf{h}_\gamma^T(r). \qquad \gamma = t,b \tag{32}$$

We may now obtain a set of algebraic equations by requiring the discretized functional to be stationary. To examine arbitrary variations about the solutions, we make the replacements $\zeta_\nu \to \zeta_\nu + \delta\tilde{\zeta}_\nu$ and $\chi_\nu \to \chi_\nu + \delta\tilde{\chi}_\nu$ in Eqs. (21) and (22). Requiring the linear term in δ to vanish yields

$$\mathbf{A}_\nu \zeta_\nu + \mathbf{M}_\nu \chi_\nu = \mathbf{s}_\nu. \tag{33}$$

Requiring the linear term in ε to vanish imposes continuity across nodal interfaces of the moments defined by

$$\psi_\nu = \mathbf{M}_\nu^T \zeta_\nu. \tag{34}$$

We may solve Eq. (33) for ζ_ν,

$$\zeta_\nu = \mathbf{A}_\nu^{-1}\mathbf{s}_\nu - \mathbf{A}_\nu^{-1}\mathbf{M}_\nu \chi_\nu, \tag{35}$$

and combine the result with Eq. (34) to obtain

$$\psi_\nu = \mathbf{M}_\nu^T \mathbf{A}_\nu^{-1}\mathbf{s}_\nu - \mathbf{M}_\nu^T \mathbf{A}_\nu^{-1}\mathbf{M}_\nu \chi_\nu. \tag{36}$$

At this point, we have written the even-parity flux moments ψ_ν at the node interface in terms of the source and the odd-parity interface moments χ_ν, while imposing the continuity of both of these moments between neighboring nodes. The final step is to transform variables such that Eq. (36) may be written in terms of a response matrix. Introducing the partial current-like variables

$$\mathbf{j}_\nu^\pm = \tfrac{1}{4}\psi_\nu \pm \tfrac{1}{2}\chi_\nu \tag{37}$$

into Eq. (39) and (40) then yields response matrix equation for each node:

$$\mathbf{j}_\nu^+ = \mathbf{R}_\nu \mathbf{j}_\nu^- + \mathbf{B}_\nu \mathbf{s}_\nu, \tag{38}$$

where $\mathbf{R}_\nu = \left(\tfrac{1}{2}\mathbf{M}_\nu^T \mathbf{A}_\nu^{-1}\mathbf{M}_\nu + \mathbf{I}\right)^{-1}\left(\tfrac{1}{2}\mathbf{M}_\nu^T \mathbf{A}_\nu^{-1}\mathbf{M}_\nu - \mathbf{I}\right)$ and $\mathbf{B}_\nu = \left(\tfrac{1}{2}\mathbf{M}_\nu^T \mathbf{A}_\nu^{-1}\mathbf{M}_\nu + \mathbf{I}\right)^{-1}\tfrac{1}{2}\mathbf{M}_\nu^T \mathbf{A}_\nu^{-1}$.

3. Results

The *R-Z* formalism is being implemented as a modification of the multigroup VARIANT code at Argonne National Laboratory, for both diffusion theory and higher-order spherical harmonics

calculations. Both fixed source and eigenvalue options are included. To test the fixed source capability the well-known Iron-water problem [5] has been recast from *X-Y* to *R-Z* geometry, with all dimensions and cross sections remaining the same. Figures 3 and 4 show P_1 and P_3 results close to the vacuum boundaries. Fine meshes with $\Delta r = \Delta z = 1$ cm, and a coarse mesh, with $\Delta r = \Delta z = 3$ cm, are presented. For comparison, fine mesh x-y calculations are also included. The substantial transport effects are, as expected, present in *R-Z* as well as *X-Y* geometry.

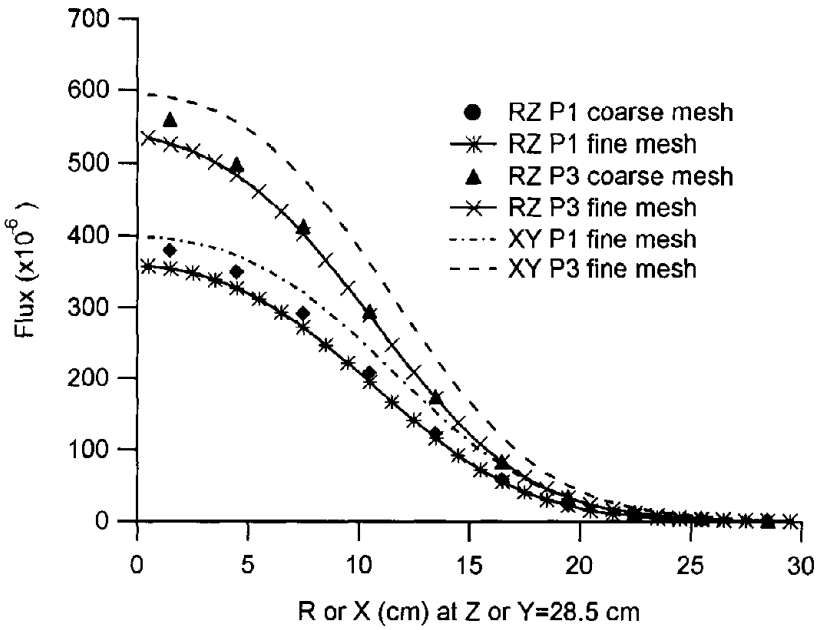

Fig. 3 Flux distribution close to the vacuum boundary on the top for the Iron-water problem

To examine spatial truncation errors, we utilize two-group eigenvalue problems. Table 1 provides P_l eigenvalue results using two group MOX fuel and water cross sections. The core is 40 cm in radius and 80 cm in height surrounded by radial and axial reflectors 20 cm thick. A reflected boundary condition is used to reduce the modeling to the upper half of the core. The eigenvalue is tabulated vs. both *h* and *p* refinement. Aside from the coarsest nodes, the accuracy increases faster with *p* refinement (i.e. increasing the polynomial order in the interface approximation) than in reducing the mesh size in *h* refinement. Moreover, both CPU time and memory requirements increase substantially with mesh size reduction, but much less so with increased polynomial order.

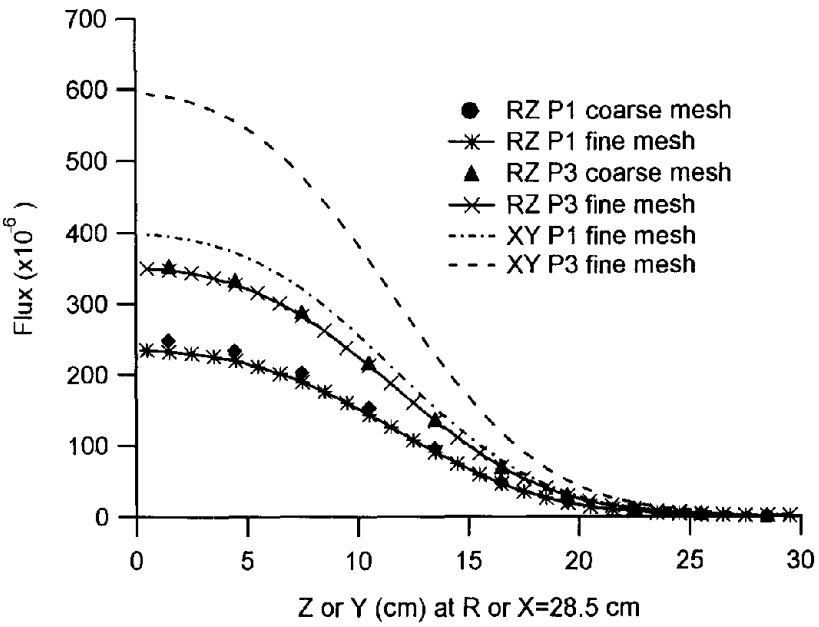

Fig. 4 Flux distribution close to the vacuum boundary on the right for the Iron-water problem

Interface / Δr & Δz	Flat	Linear	Quadratic
10cm	0.95450 (1.21×10^{-1}%)	0.95349 (1.47×10^{-2}%)	0.95349 (1.47×10^{-2}%)
4cm	0.95351 (1.68×10^{-2}%)	0.95335 (0.00%)	0.95335 (0.00%)
2cm	0.95339 (3.15×10^{-3}%)	0.95335 (0.00%)	0.95335 (0.00%)
1cm	0.95336 (1.05×10^{-3}%)	0.95335 (0.00%)	0.95335 (0.00%)

Table 1 Comparison of *h*-refinement and *p*-refinement for Two-Region Eigenvalue Problem

4. Conclusions

The foregoing results demonstrate the ability of the variational nodal method to treat problems in R-Z geometry. The curvilinear coordinate system, however, presents two challenges that are not present in Cartesian geometry. First, the central elements must be treated specifically, and the trial functions constrained to assure that the appropriate symmetry conditions on the angular flux are met along the center line. Second, each radial response matrix must be calculated separately, for there is no

translational invariance in the radial direction; each radial node corresponds to a toroid with a unique radius.

Acknowledgements

This work was supported, in part, through Department of Energy contracts DE-FG07-01: ID14106 & ID14108.

References

1. G. Palmiotti, E. E. Lewis & C. B. Carrico, "VARIANT: VARIational Anisotropic Nodal Transport for Multidimensional Cartesian and Hexagonal Geometry Calculation," Argonne National Laboratory ANL-95/40, 1995.
2. E. E. Lewis, C. B. Carrico and G. Palmiotti, "Variational Nodal Formulation for the Spherical Harmonics Equations," Nucl. Sci. Eng., 122, 194-203, 1996
3. R. Douglas O'Dell and Raymond E. Alcouffe, "Transport Calculation for Nuclear Analyses: Theory and Guidelines for Effective Use of Transport Codes," Los Alamos National Laboratory LA-10983-MS, 1987
4. E. E. Lewis and W. F. Miller, Jr., "Computational Methods of Neutron Transport," John Wiley & Sons, New York, 1984
5. E. M. Gelbard, "Argonne Code Center: Benchmark Problem Book," ANL-7416 Supplement 1 Mathematics and Computers, Argonne National Laboratory, 1972

Appendix C

Submitted to *Nucl. Sci. Eng.*

Generalization of the Variational Nodal Method to Spherical Harmonics Approximations in R-Z Geometry

Hui Zhang & E. E. Lewis*
Northwestern University
Department of Mechanical Engineering
Evanston, IL 60208 USA

Abstract-The variational nodal method is generalized to include *R-Z* geometry. Spherical harmonic trial functions in angle are combined with orthonormal polynomials in space to discretize the multigroup equations. The response matrices that result correspond to nodal volumes that are toroids, with rectangular cross sections, except along centerline where they are cylinders. The *R-Z* response matrix equations are implemented as modifications to the Argonne National Laboratory code, VARIANT, and existing iterative methods are used to obtain numerical solutions. The method is tested in t P_1, P_3, and P_5 approximations and results are presented for both a one-group fixed source and a two-group eigenvalue problem.

1. Introduction

The variational nodal method has found substantial use in both diffusion theory and higher-order spherical harmonics approximations for a variety of reactor physics problems.[1-4] The method, as implemented in the Argonne National Laboratory code, VARIANT,[4] has been available in both two- and three-dimensional Cartesian and hexagonal geometries. However, the need sometimes arises for two-dimensional *R-Z* geometry calculations, particularly for scoping studies, where transport effects may be significant, but where the expense of three-dimensional transport calculations is not warranted.

Two challenges not present in Cartesian co-ordinates present themselves in *R-Z* transport methods:[5,6] the coupling of spatial and angular trial functions through the angular derivative in the gradient operator, and the need to impose an angular symmetry condition on the trial functions along the centerline. Moreover the resulting response matrix domains take the form of toroids with rectangular cross sections, except along the centerline where they are cylinders. In the following section we employ spherical harmonics in angle and polynomial trial functions in space to obtain the *R-Z* response matrices within the framework of the variational nodal method. We implement the resulting formulation as a modification of the VARIANT code, and then in section 3 we present results for both a fixed-source problem, which is a *R-Z* modification of the iron-water benchmark, and to a two group eigenvalue problem. The paper concludes with a brief discussion.

* Corresponding author, Tel. 847-491-3579, FAX 847-491-3915, E-mail: e-lewis@northwestern.edu

2. Theory

2.1 Variational Formulation

The variational nodal method is a primal hybrid finite element representation of the even-parity form of the transport equation. In the hybrid formulation, the problem domain V is decomposed into subdomains V_ν (also called elements or nodes):

$$V = \sum_\nu V_\nu . \tag{1}$$

Within each node, the even-parity form of the within-group transport equation is solved in space ($\vec{r}$) and angle ($\hat{\Omega}$):

$$-\hat{\Omega}\cdot\vec{\nabla}\sigma^{-1}\hat{\Omega}\cdot\vec{\nabla}\psi^+(\vec{r},\hat{\Omega})+\sigma\,\psi^+(\vec{r},\hat{\Omega})=\sigma_s\int d\hat{\Omega}'\psi^+(\vec{r},\hat{\Omega}')+s(\vec{r}),\quad \vec{r}\in V_\nu \tag{2}$$

where ψ^+ is the even parity flux component, σ and σ_s the total and scattering cross sections and s the group source. Isotropic scattering and sources are assumed. The odd-parity flux ψ^-, which is related to ψ^+ by

$$\hat{\Omega}\cdot\vec{\nabla}\psi^+(\vec{r},\hat{\Omega})+\sigma\psi^-(\vec{r},\hat{\Omega})=0,\qquad \vec{r}\in\Gamma_\nu \tag{3}$$

is defined only along the node interface Γ_ν as a Lagrange multiplier.

The functional for the variational nodal method is given as a superposition of nodal contributions:

$$F[\psi^+,\psi^-]=\sum_\nu F_\nu[\psi^+,\psi^-], \tag{4}$$

where

$$F_\nu[\psi^+,\psi^-]=\int_\nu dV\left\{\int d\hat{\Omega}[\sigma^{-1}(\hat{\Omega}\cdot\vec{\nabla}\psi^+)^2+\sigma\psi^{+2}]-\sigma_s\phi^2-2\phi s\right\}+2\int_\nu d\Gamma\int d\hat{\Omega}\hat{\Omega}\cdot\hat{n}\psi^+\psi^-, \tag{5}$$

and ϕ is the scalar flux. We require this functional to be stationary with respect to arbitrary variations $\tilde{\psi}^+$ and $\tilde{\psi}^-$ about the true solutions ψ^+ and ψ^-. Thus, we make the replacements $\psi^+\to\psi^+ +\delta\tilde{\psi}^+$ and $\psi^-\to\psi^- +\varepsilon\tilde{\psi}^-$ where δ and ε are small positive constants, and require the linear terms in δ and ε to vanish. Setting the linear term in δ to zero yields the weak form of Eq. (2):

$$\int_\nu dV\int d\hat{\Omega}[\sigma^{-1}(\hat{\Omega}\cdot\vec{\nabla}\tilde{\psi}^+)(\hat{\Omega}\cdot\vec{\nabla}\psi^+)+\tilde{\psi}^+(\sigma\psi^+-\sigma_s\phi-s)]+\int_\nu d\Gamma\int d\hat{\Omega}\hat{\Omega}\cdot\hat{n}\tilde{\psi}^+\psi^-=0. \tag{6}$$

Applying the divergence theorem then yields

$$\int_V dV \int d\Omega \tilde{\psi}^+ (-\hat{\Omega}\cdot\vec{\nabla}\sigma^{-1}\hat{\Omega}\cdot\vec{\nabla}\psi^+ + \sigma\psi^+ - \sigma_s\phi - s) + \int_V d\Gamma \int d\Omega\hat{\Omega}\cdot\hat{n}\tilde{\psi}^+(\psi^- + \sigma^{-1}\hat{\Omega}\cdot\vec{\nabla}\psi^+) = 0. \qquad (7)$$

Clearly, Eq. (2) must be satisfied if the volume integral is to vanish for arbitrary $\tilde{\psi}^+$. In addition, Eq. (3) must be met at the interface for the surface integral to vanish. The continuity conditions across nodal interfaces may be stated as follows. Since the Lagrange multiplier ψ^- and its variation $\tilde{\psi}^-$ are uniquely defined at the interface, two conditions are imposed. First, the surface integral in Eq. (7) imposes continuity on $\sigma^{-1}\hat{\Omega}\cdot\vec{\nabla}\psi^+$. Second, requiring the linear term in ε to vanish yields for each nodal interface, say between nodes V_ν and $V_{\nu'}$, a condition of the form

$$\int_V d\Gamma \int d\Omega\hat{\Omega}\cdot\hat{n}\tilde{\psi}^-(\psi^+ - \psi'^+) = 0, \qquad (8)$$

since $\hat{n}_\nu = -\hat{n}_{\nu'}$. Thus ψ^+ must be continuous across the interface.

2.2. Cylindrical Coordinates (r, z)

The *R-Z* cylindrical coordinates system is shown in Figure 1, together with an angular-direction coordinates system used to define the particle direction $\hat{\Omega}$. In this system, a spatial point is defined by its (r, z) coordinate , while $\hat{\Omega}$ is defined by

$$\hat{\Omega} = \Omega_r\hat{r} + \Omega_\omega\hat{\omega} + \Omega_z\hat{z}, \qquad (9)$$

where

$$\begin{aligned} \Omega_r &= (1-\mu^2)^{1/2}\cos\omega, \\ \Omega_\omega &= (1-\mu^2)^{1/2}\sin\omega, \\ \Omega_z &= \mu \end{aligned} \qquad (10)$$

with $\mu = \cos\theta$. The $\hat{\Omega}\cdot\vec{\nabla}$ may be determined by [5,6]

$$\hat{\Omega}\cdot\vec{\nabla} = \Omega_r\frac{\partial}{\partial r} - \frac{1}{r}\Omega_\omega\frac{\partial}{\partial\omega} + \Omega_z\frac{\partial}{\partial z}, \qquad (11)$$

and the incremental angle is defined as $d\Omega = (4\pi)^{-1}d\mu d\omega$.

2.3. Discretization

We begin by considering a rectangular node in *r, z* bounded on left and right by $r_l \le r \le r_r$ and on bottom and top by $z_b \le z \le z_t$ as shown in Figure 2. We expand the even-parity flux coefficients within the node as

$$\psi^+(r,z,\hat{\Omega}) = \mathbf{g}^T(\hat{\Omega})\otimes\mathbf{f}^T(r,z)\xi_\nu. \qquad r_l \le r \le r_r, z_b \le z \le z_t \quad (12)$$

Here $\otimes$ denotes the Kronecker product, and $\mathbf{g}(\hat{\Omega})$ is a vector of even-order spherical harmonics with M terms obeying the orthonormal condition

$$\int d\Omega \mathbf{g}(\hat{\Omega})\mathbf{g}^T(\hat{\Omega}) = \mathbf{I}_M . \tag{13}$$

The I spatial trial functions constituting the vecttor $\mathbf{f}(r,z)$ form a complete polynomial. They are Legendre polynomials in z and also constructed to be orthogonal in r, such that

$$\frac{1}{V_v}\int_v dV \mathbf{f}(r,z)\mathbf{f}^T(r,z) = \mathbf{I}_I , \tag{14}$$

In R-Z geometry, $V_v = 2\pi(r_r^2 - r_l^2)(z_t - z_b)$ and

$$\int_v dV(\cdot) = 2\pi \int_{r_l}^{r_r} dr r \int_{z_b}^{z_t} dz(\cdot) \tag{15}$$

The vector ξ_v in Eq, (12) contains the unknown coefficients.

Along the node interfaces, we make the expansions

$$\psi^-(\vec{r},\hat{\Omega}) = \mathbf{k}_\gamma^T(\hat{\Omega}) \otimes h_\gamma^T(z)\chi_\gamma^{'}, \qquad \vec{r} \in \Gamma_r, \Gamma_l$$

and $\tag{16}$

$$\psi^-(\vec{r},\hat{\Omega}) = \mathbf{k}_\gamma^T(\hat{\Omega}) \otimes h_\gamma^T(r)\chi_\gamma^{'}, \qquad \vec{r} \in \Gamma_t, \Gamma_b$$

where $\mathbf{k}_\gamma(\hat{\Omega})$ is vector of odd-order spherical harmonics with N terms in which the angular coordinates have been rotated such that the polar angle, $\mu = \hat{\Omega}\cdot\hat{n}_\gamma$, is taken with respect to the surface normal. They obey the orthonormal conditions

$$\int d\Omega \mathbf{k}_\gamma(\hat{\Omega})\mathbf{k}_\gamma^T(\hat{\Omega}) = \mathbf{I}_N$$

and $\qquad \gamma = r,t,l,b \tag{17}$

$$\int d\Omega \mathbf{g}(\hat{\Omega})\mathbf{k}_\gamma^T(\hat{\Omega}) = \mathbf{0}$$

The spatial trial functions $\mathbf{h}_\gamma$ are set sets of orthogonal polynomials defined along the interfaces.

The source and the scalar flux may be approximated as

$$\mathbf{s} = \mathbf{w}s(r,z) \tag{18}$$

and $\qquad r_l \le r \le r_r, z_b \le z \le z_t$

$$\phi(\vec{r}) = \mathbf{w}^T \otimes \mathbf{f}^T(r,z)\xi_v \tag{19}$$

with $[\mathbf{w}]_m = \delta_{m1}$.

The nodal volumes corresponding to the response matrices will be toroids with rectangular cross sections in the r, z plane. The central nodes, however, are cylinders with three surfaces. The centerline symmetry condition that the angular flux be independent of the azimuthal angle. Thus,

$$\lim_{r\to 0}\psi^+(\vec{r},\hat{\Omega}) = \psi^+(z,\theta).$$

This symmetry condition requires that the central nodes contain two sets of trial functions for ψ^+ when spherical harmonics are employed. Therefore, for the central element we expand the even-parity flux within the node as

$$\Psi^+(\vec{r},\hat{\Omega}) = \left[\mathbf{g}^{0T}\otimes\mathbf{f}^{eT}\ \ \mathbf{g}^{1T}\otimes\mathbf{f}^{oT}\right]\xi_v, \qquad r_l \le r \le r_r, z_b \le z \le z_t \quad (20)$$

where $\mathbf{f}^e$ are the spatial trial function sets including only even functions in r for the Y_{l0} terms in $\mathbf{g}^0$, which are independent of ω, causing the radial derivative vanishes at $r = 0$; $\mathbf{f}^o$ are the spatial trial function sets including only odd functions of r for the ω dependent Y_{lm}, $m \neq 0$ terms in $\mathbf{g}^1$. Hence the terms in $\mathbf{f}^o$ vanish at the origin. The two spatial trial function sets $\mathbf{f}^e$ and $\mathbf{f}^o$ contain I^e and I^o spatial polynomial trial functions, respectively, and meet the orthogonality condition

$$\frac{1}{V_v}\int_v dV\mathbf{f}^e(r,z)\mathbf{f}^{eT}(r,z) = \mathbf{I}_{I^e},$$

and (21)

$$\frac{1}{V_v}\int_v dV\mathbf{f}^o(r,z)\mathbf{f}^{oT}(r,z) = \mathbf{I}_{I^o}.$$

The two sets of angular trial function $\mathbf{g}^0$ and $\mathbf{g}^1$ consist of M^o and M^e terms, respectively, and obey the orthonormal conditions

$$\int d\Omega\mathbf{g}^o(\hat{\Omega})\mathbf{g}^{oT}(\hat{\Omega}) = \mathbf{I}_{M^o},$$

and (22)

$$\int d\Omega\mathbf{g}^e(\hat{\Omega})\mathbf{g}^{eT}(\hat{\Omega}) = \mathbf{I}_{M^e}.$$

With these stipulations, the singularities that would otherwise be encountered in applying the operator of Eq. (11) are removed. Note, also, that unlike Cartesian geometry, each response matrix in the radial direction is unique, even though the cross sections and the widths and heights of the nodes are same.

2.4. Response Matrix Evaluation

Response matrices are obtained from the foregoing space-angle trial functions by inserting them into Eqs. (4) and (5). This reduces the functional to the algebraic form:

$$F=\sum_{\nu}F_{\nu}[\zeta_{\nu},\chi_{\nu}] \tag{23}$$

and

$$F_{\nu}[\zeta_{\nu},\chi_{\nu}]=\zeta_{\nu}^{T}\mathbf{A}_{\nu}\zeta_{\nu}-2\zeta_{\nu}^{T}\mathbf{s}_{\nu}+2\zeta_{\nu}^{T}\mathbf{M}_{\nu}\chi_{\nu}. \tag{24}$$

Each of the elements of $\mathbf{A_V}$ is given in terms of integrals over known spatial or angular trial functions. The matrix $\mathbf{A_V}$ for non-central elements is given as

$$\mathbf{A}_{\nu}=\sigma_{\nu}^{-1}\mathbf{H}_{kk'}\otimes\int_{\nu}dV(\nabla_{k}\mathbf{f})(\nabla_{k'}\mathbf{f}^{T})+(\sigma_{\nu}\mathbf{I}_{M}-\sigma_{s\nu}\mathbf{w}\mathbf{w}^{T})\otimes V_{\nu}\mathbf{I}_{I}, \tag{25}$$

where repeated subscripts k or k' indicates summation with $k,k'=r,\omega,z$, and

$$\begin{aligned}\nabla_{r}\mathbf{f}&=\partial\mathbf{f}/\partial r,\\ \nabla_{\omega}\mathbf{f}&=\mathbf{f}/r,\\ \nabla_{z}\mathbf{f}&=\partial\mathbf{f}/\partial z,\end{aligned} \tag{26}$$

$$\mathbf{H}_{kk'}=\int d\Omega\Omega_{k}\Omega_{k'}\breve{\mathbf{g}}_{k}\breve{\mathbf{g}}_{k'}^{T}, \tag{27}$$

with

$$\breve{\mathbf{g}}_{r,z}=\mathbf{g}, \tag{28}$$

and

$$\breve{\mathbf{g}}_{\omega}=-\partial\mathbf{g}/\partial\omega.$$

The incremental spatial volume is given by $dV=2\pi r dr dz$. The matrix $\mathbf{A_V}$ for central elements is given as

$$A_{\nu}=\sigma^{-1}\begin{bmatrix}\mathbf{H}_{kl}^{1,1}\otimes\mathbf{P}_{kl}^{1,1} & \mathbf{H}_{kl}^{1,2}\otimes\mathbf{P}_{kl}^{1,2}\\ \mathbf{H}_{kl}^{2,1}\otimes\mathbf{P}_{kl}^{2,1} & \mathbf{H}_{kl}^{2,2}\otimes\mathbf{P}_{kl}^{2,2}\end{bmatrix}+\sigma_{\nu}\otimes\mathbf{I}_{M^{e}\times I^{e}+M^{o}\times I^{o}}-\sigma_{s\nu}\otimes\mathbf{w}\mathbf{w}^{T}\mathbf{I}_{I} \tag{29}$$

where

$$\begin{aligned}\mathbf{H}_{kl}^{1,1}&=\int d\Omega\Omega_{k}\Omega_{l}\breve{\mathbf{g}}_{k}^{0}\breve{\mathbf{g}}_{l}^{0T},\\ \mathbf{H}_{kl}^{1,2}&=\int d\Omega\Omega_{k}\Omega_{l}\breve{\mathbf{g}}_{k}^{0}\breve{\mathbf{g}}_{l}^{1T},\\ \mathbf{H}_{kl}^{2,1}&=\int d\Omega\Omega_{k}\Omega_{l}\breve{\mathbf{g}}_{k}^{1}\breve{\mathbf{g}}_{l}^{0T},\\ \mathbf{H}_{kl}^{2,2}&=\int d\Omega\Omega_{k}\Omega_{l}\breve{\mathbf{g}}_{k}^{1}\breve{\mathbf{g}}_{l}^{1T},\end{aligned} \tag{30}$$

and

$$\begin{aligned}\mathbf{P}_{kl}^{1,1}&=\int dV\nabla_{k}\mathbf{f}^{e}\nabla_{l}\mathbf{f}^{eT},\\ \mathbf{P}_{kl}^{1,2}&=\int dV\nabla_{k}\mathbf{f}^{e}\nabla_{l}\mathbf{f}^{oT},\\ \mathbf{P}_{kl}^{2,1}&=\int dV\nabla_{k}\mathbf{f}^{o}\nabla_{l}\mathbf{f}^{eT},\\ \mathbf{P}_{kl}^{2,2}&=\int dV\nabla_{k}\mathbf{f}^{o}\nabla_{l}\mathbf{f}^{oT}.\end{aligned} \tag{31}$$

The source is

$$\mathbf{s}_v = \int_v dV \mathbf{s} \otimes \mathbf{f} . \tag{32}$$

The surface coefficients are partitioned according to the four interfaces:

$$\chi_v = \begin{bmatrix} \chi_r \\ \chi_t \\ \chi_l \\ \chi_b \end{bmatrix} \tag{33}$$

The $\mathbf{M}_v$ matrix is then given as

$$\mathbf{M}_v = \left[\mathbf{M}'_r, \mathbf{M}'_t, \mathbf{M}'_l, \mathbf{M}'_b\right], \tag{34}$$

For non-central elements

$$\mathbf{M}'_\gamma = \mathbf{E}_\gamma \otimes \mathbf{D}_\gamma, \qquad \gamma = r,t,l,b \tag{35}$$

where

$$\vec{\mathbf{E}}_\gamma = \int d\Omega \hat{\Omega} \cdot \hat{n}_\gamma \mathbf{g}(\hat{\Omega}) \mathbf{k}_\gamma^T(\hat{\Omega}) , \tag{36}$$

and

$$\mathbf{D}_\gamma = 2\pi r_\gamma \int_{z_b}^{z_t} dz \mathbf{f}(r_\gamma, z) \mathbf{h}_\gamma^T(z) , \qquad \gamma = r,l \tag{37}$$

$$\mathbf{D}_\gamma = 2\pi \int_{r_l}^{r_r} dr r \mathbf{f}(r, z_\gamma) \mathbf{h}_\gamma^T(r) . \qquad \gamma = t,b$$

For central elements

$$\mathbf{M}'_\gamma = \begin{bmatrix} \mathbf{E}_\gamma^0 \otimes \mathbf{D}_\gamma^e \\ \mathbf{E}_\gamma^1 \otimes \mathbf{D}_\gamma^o \end{bmatrix}, \tag{38}$$

where

$$\mathbf{E}_\gamma^0 = \int d\Omega \hat{\Omega} \cdot \hat{n} \mathbf{g}^0 \mathbf{k}_\gamma^T , \tag{39}$$
$$\mathbf{E}_\gamma^1 = \int d\Omega \hat{\Omega} \cdot \hat{n} \mathbf{g}^1 \mathbf{k}_\gamma^T ,$$

and

$$\mathbf{D}_\gamma^e = 2\pi r_\gamma \int_\gamma dz \mathbf{f}^e(r_\gamma, z) \mathbf{h}_\gamma^T(z), \quad \gamma = l,r ,$$

$$\mathbf{D}_\gamma^e = 2\pi \int_\gamma dr r \mathbf{f}^e(r, z_\gamma) \mathbf{h}_\gamma^T(r), \quad \gamma = b,t , \tag{40}$$

$$\mathbf{D}_\gamma^o = 2\pi r_\gamma \int_\gamma dz \mathbf{f}^o(r_\gamma, z) \mathbf{h}_\gamma^T(z), \quad \gamma = l,r ,$$

$$\mathbf{D}_\gamma^o = 2\pi \int_\gamma dr r \mathbf{f}^o(r, z_\gamma) \mathbf{h}_\gamma^T(r), \quad \gamma = b,t .$$

We may now obtain a set of algebraic equations by requiring the discretized functional to be stationary. To examine arbitrary variations about the solutions, we make the replacements $\zeta_\nu \to \zeta_\nu + \delta\tilde{\zeta}_\nu$ and $\chi_\nu \to \chi_\nu + \delta\tilde{\chi}_\nu$ in Eqs. (23) and (24). Requiring the linear term in δ to vanish yields

$$\mathbf{A}_\nu \zeta_\nu + \mathbf{M}_\nu \chi_\nu = \mathbf{s}_\nu . \tag{41}$$

Requiring the linear term in ε to vanish imposes continuity across nodal interfaces of the moments defined by

$$\psi_\nu = \mathbf{M}_\nu^T \zeta_\nu . \tag{42}$$

We may solve Eq. (41) for ζ_ν,

$$\zeta_\nu = \mathbf{A}_\nu^{-1}\mathbf{s}_\nu - \mathbf{A}_\nu^{-1}\mathbf{M}_\nu \chi_\nu , \tag{43}$$

and combine the result with Eq. (42) to obtain

$$\psi_\nu = \mathbf{M}_\nu^T \mathbf{A}_\nu^{-1}\mathbf{s}_\nu - \mathbf{M}_\nu^T \mathbf{A}_\nu^{-1}\mathbf{M}_\nu \chi_\nu . \tag{44}$$

At this point, we have written the even-parity flux moments ψ_ν at the node interface in terms of the source and the odd-parity interface moments χ_ν, while imposing the continuity of both of these moments between neighboring nodes. The final step is to transform variables such that Eq. (36) may be written in terms of a response matrix. Introducing the partial current-like variables

$$\mathbf{j}_\nu^{\pm} = \tfrac{1}{4}\psi_\nu \pm \tfrac{1}{2}\chi_\nu \tag{45}$$

into Eq. (44) then yields response matrix equation for each node:

$$\mathbf{j}_\nu^{+} = \mathbf{R}_\nu \mathbf{j}_\nu^{-} + \mathbf{B}_\nu \mathbf{s}_\nu , \tag{46}$$

where $\mathbf{R}_\nu = \left(\tfrac{1}{2}\mathbf{M}_\nu^T \mathbf{A}_\nu^{-1}\mathbf{M}_\nu + \mathbf{I}\right)^{-1}\left(\tfrac{1}{2}\mathbf{M}_\nu^T \mathbf{A}_\nu^{-1}\mathbf{M}_\nu - \mathbf{I}\right)$ and $\mathbf{B}_\nu = \left(\tfrac{1}{2}\mathbf{M}_\nu^T \mathbf{A}_\nu^{-1}\mathbf{M}_\nu + \mathbf{I}\right)^{-1} \tfrac{1}{2}\mathbf{M}_\nu^T \mathbf{A}_\nu^{-1}$.

3. Results

The *R-Z* formalism presented herein has been implemented as a modification of the multigroup VARIANT code at Argonne National Laboratory, for both diffusion theory and higher-order spherical harmonics calculations. Both fixed source and eigenvalue options are included. To test the fixed source capability the well-known Iron-water problem[7] has been recast from *X-Y* to *R-Z* geometry, with all dimensions and cross sections remaining the same. The problem domain is composed of a source region at the center of a water pool that is surrounded by an iron shield. With reflecting boundary conditions at the left and bottom boundary, only one quarter of the physical domain is modeled. The configuration is shown in Figure 3. The three compositions, the cross section data and the source strength are given in Table 1. Figures 4 and 5 show P_1, P_3 and P_5 results close to the vacuum boundaries. Fine meshes with $\Delta r = \Delta z = 1$ cm, and a coarse mesh, with $\Delta r = \Delta z = 3$ cm, are presented.

For comparison, fine mesh x-y calculations are also included. The substantial transport effects are, as expected, present in *R-Z* as well as *X-Y* geometry.

To test the multigroup eigenvalue formulation and to examine spatial truncation errors, we utilize two-region two-group eigenvalue problems. Table 2 provides P_1, P_3, and P_5 eigenvalue results using two group MOX fuel and water cross sections. The geometry is given in Figure 6. The core is 40 cm in radius and 80 cm in height surrounded by radial and axial reflectors 20 cm thick. A reflected boundary condition is used to reduce the modeling to the upper half of the core. The cross section data and neutrons per fission for the two regions and the two groups are summarized in Table 1, where σ_t is the microscopic total cross section, σ_γ is the microscopic capture cross section, σ_f is the microscopic fission cross section, σ_s is the microscopic scattering cross section, and ν is the neutrons per fission. The eigenvalue is tabulated vs. both *h* and *p* refinement where the eigenvalue result (K=0.954186) from P_5 with 2cm nodal grid was taken as the reference result. Aside from the coarsest nodes, the accuracy increases faster with *p* refinement (i.e. increasing the polynomial order in the interface approximation) than in reducing the mesh size in *h* refinement. Moreover, both CPU time and memory requirements increase substantially with mesh size reduction, but much less so with increased polynomial order. For comparison, a MCNP Monte Carlo calculation has been performed yielding a result of K=0.95420 ± 0.00055 at 68% confidence level. A 2cm grid TWODANT S_{16} calculation was also performed, yielding K=0.95455.

4. Discussion

The foregoing results demonstrate the ability of the variational nodal method to treat problems in R-Z geometry. The curvilinear coordinate system, however, presents two challenges that are not present in Cartesian geometry. First, the central elements must be treated specifically, and the trial functions constrained to assure that the appropriate symmetry conditions on the angular flux are met along the center line. Second, each radial response matrix must be calculated separately, for there is no translational invariance in the radial direction; each radial node corresponds to a toroid with a unique radius.

Acknowledgements

This work was supported, in part, through Department of Energy contracts DE-FG07-01: ID14106 & ID14108. Michael A. Smith of Argonne National Laboratory provided the MCNP and TWODANT results.

References

1. C. B. Carrico, E. E. Lewis and G. Palmiotti, " Three-Dimensional Variational Nodal Transport Methods for Cartesian, Triangular and Hexagonal Criticality Calculations," *Nucl. Sci. Eng.* **111**, 168-179 (1992).

2. G. Palmiotti ,C. B. Carrico, and E. E. Lewis, "Variational Nodal Transport Methods with Anisotropic Scattering," *Nucl. Sci. Eng.*, **115**, 223 (1993).
3. E. E. Lewis, C.B. Carrico and G. Palmiotti, "Variational Nodal Formulation for the Spherical Harmonics Equations," *Nucl. Sci. Eng.*, **122**, 194 (1996).
4. G. Palmiotti, E. E. Lewis & C. B. Carrico, "VARIANT: VARIational Anisotropic Nodal Transport for Multidimensional Cartesian and Hexagonal Geometry Calculation," Argonne National Laboratory ANL-95/40, 1995.
5. R. Douglas O'Dell and Raymond E. Alcouffe, "Transport Calculation for Nuclear Analyses: Theory and Guidelines for Effective Use of Transport Codes," Los Alamos National Laboratory LA-10983-MS, 1987
6. E. E. Lewis and W. F. Miller, Jr., "Computational Methods of Neutron Transport," John Wiley & Sons, New York, 1984
7. E. M. Gelbard, "Argonne Code Center: Benchmark Problem Book," ANL-7416 Supplement 1 Mathematics and Computers, Argonne National Laboratory, 1972

Table 1 Iron-water benchmark problem description

Composition	σ cm^{-1}	σ_a cm^{-1}	$c = \sigma_s/\sigma$	S $cm^{-2}s^{-1}$
1:Water	3.33	3.31002	0.994	1.
2:Water	3.33	3.31002	0.994	0.
3:Iron	1.33	1.10523	0.831	0.

Table 2 Two-region two-group eigenvalue macroscopic cross sections (cm^{-1})

		Core: MOX		Reflector: Water	
		Group 1	Group 2	Group 1	Group 2
σ_t		0.419712	1.09019	0.424766	1.13885
σ_γ		0.0112733	0.202758	0.000304551	0.0190731
σ_f		0.0068774	0.153309	0.00000	0.00000
ν		2.88366	2.87399	0.00000	0.00000
$\sigma_{s,g\leftarrow g'}$	g	g′=1	g′=2	g′=1	g′=2
	1	0.401129	0.00000	0.373999	0.00000
	2	0.000430392	0.734121	0.0504624	1.11977

Table 3 Comparison of Eigenvalue percent error
for *h*- and *p*-refinement (K_{ref} = 0.954186)

Δr & Δz	Flat(%)	Linear(%)	Quadratic(%)	
10cm	0.0335	-0.0723	-0.0723	P_1
	0.3016	0.0465	0.0301	P_3
	0.3371	0.0449	0.0492	P_5
4cm	-0.0702	-0.0870	-0.0870	P_1
	0.0549	-0.0015	0.0013	P_3
	0.1215	-0.0031	0.0025	P_5
2cm	-0.0827	-0.0870	-0.0870	P_1
	0.0036	0.0006	0.0012	P_3
	0.0077	-0.0027	0.0000	P_5

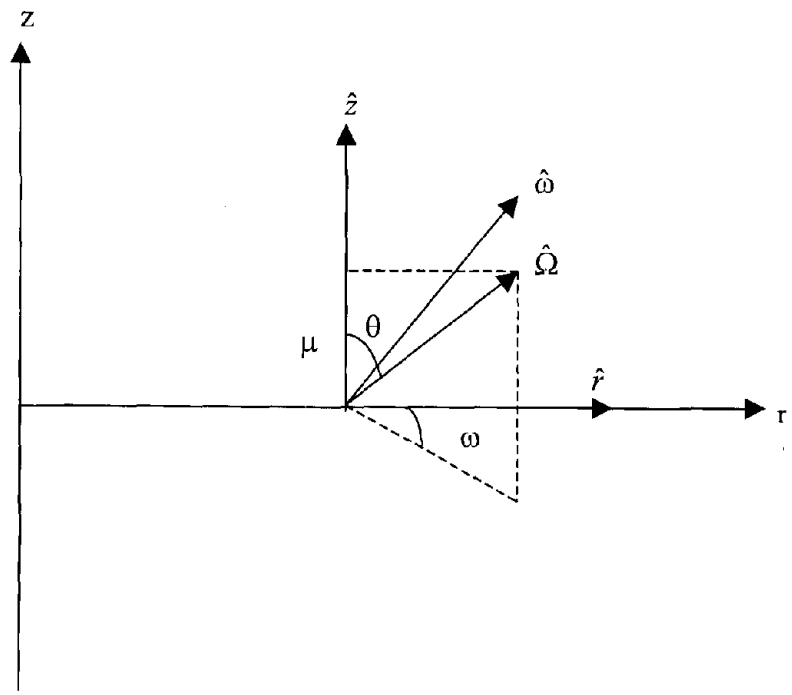

Fig. 1 Cylindrical Coordinates

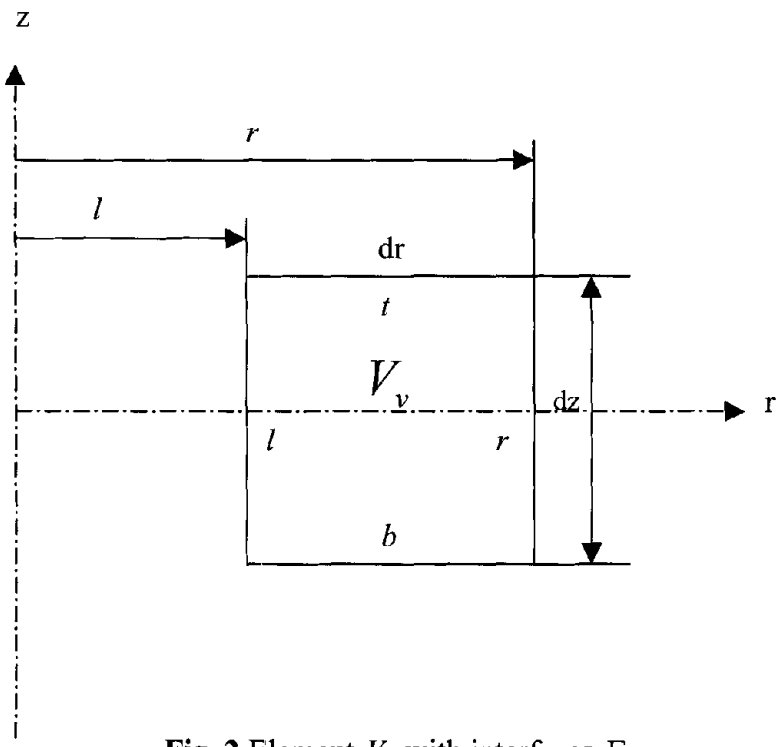

Fig. 2 Element V_v with interfaces Γ_v

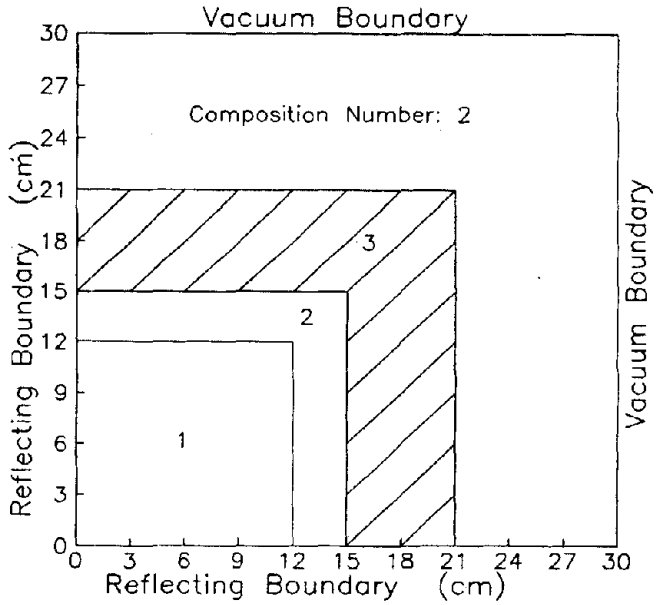

Fig. 3 Iron-Water benchmark problem configuration

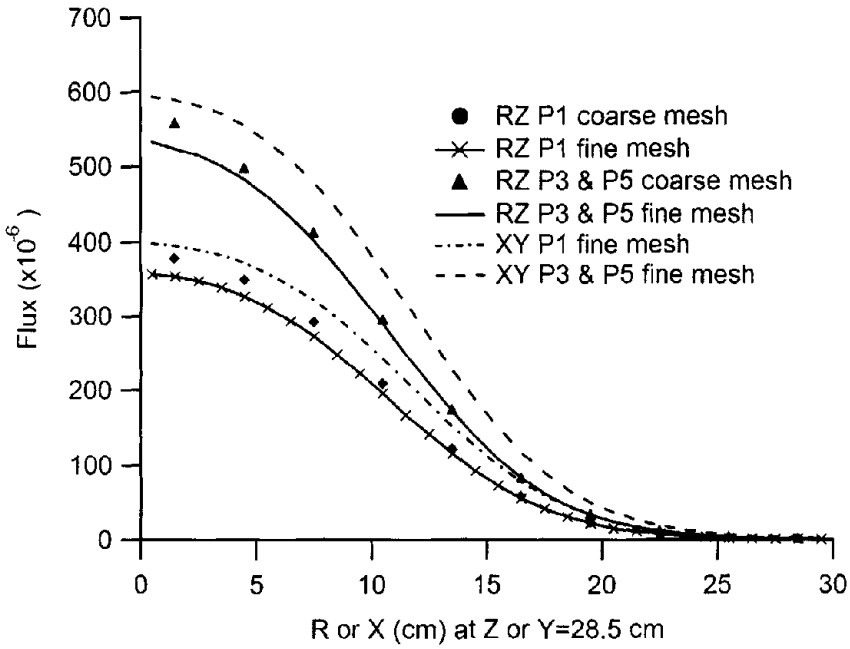

Fig. 4 Flux distribution close to the vacuum boundary on the top for the Iron-water problem

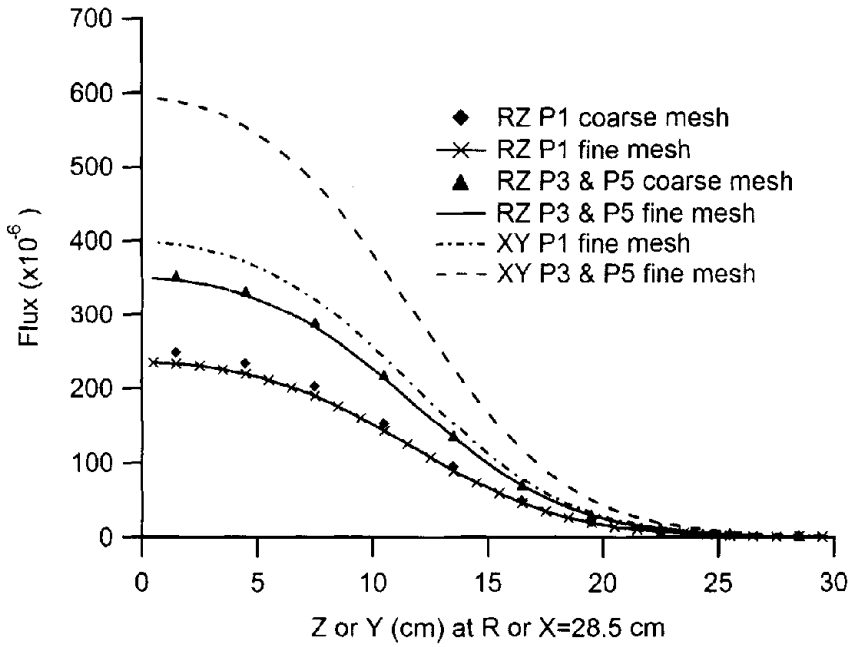

Fig. 5 Flux distribution close to the vacuum boundary on the right for the Iron-water problem

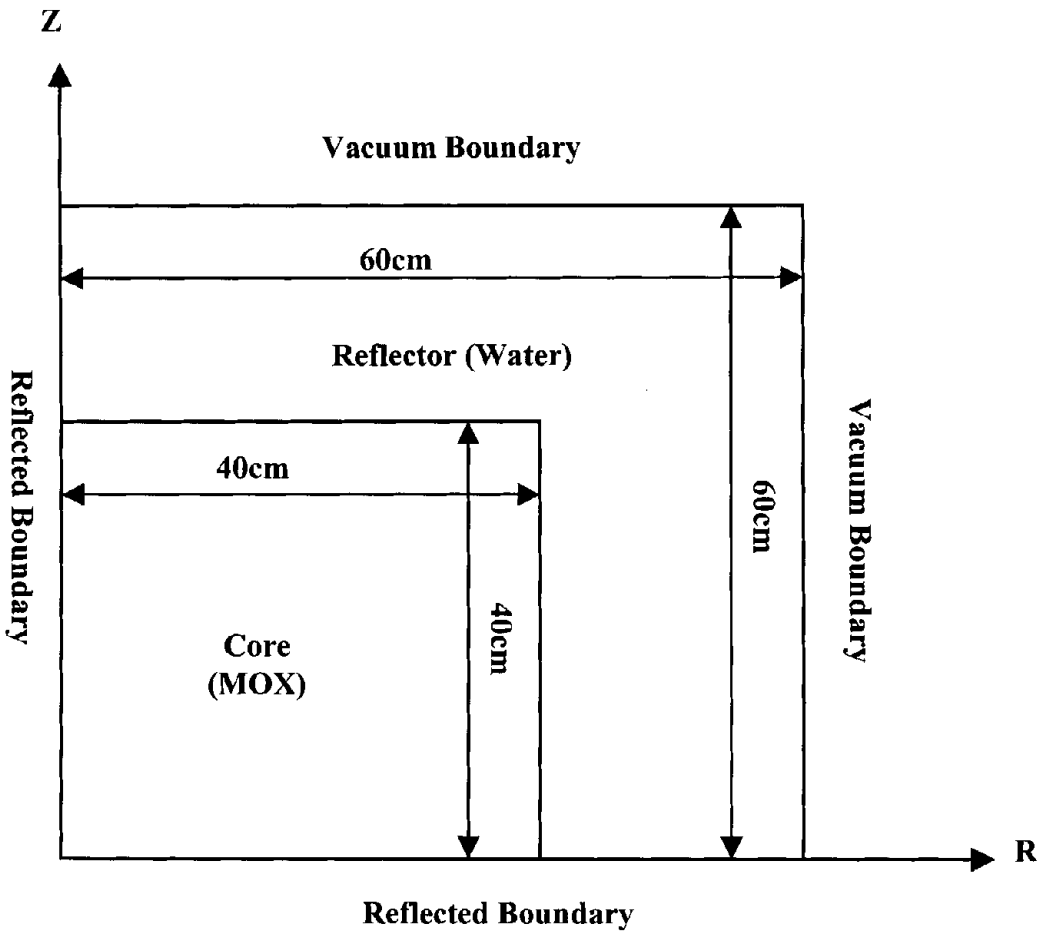

Fig. 6 Two-region eigenvalue problem configuration

PHYSOR 2004 -The Physics of Fuel Cycles and Advanced Nuclear Systems: Global Developments
Chicago, Illinois, April 25-29, 2004, on CD-ROM, American Nuclear Society, Lagrange Park, IL. (2004)

A First-Order Spherical Harmonics Formulation Compatible with the Variational Nodal Method

M. A. Smith[1], E. E. Lewis[2], G. Palmiotti[1] and W. S. Yang[1]
[1]*Argonne National Laboratory, 9700 South Cass Avenue, Argonne, Illinois 60439*
[2]*Northwestern University, Department of Mechanical Engineering, Evanston, Illinois 60208*

A spherical harmonics method based upon the first-order transport equation is formulated and implemented into VARIANT [1,2], a variational nodal transport code developed at Argonne National Laboratory. The spatial domain is split into hybrid finite elements, called nodes, where orthogonal polynomial spatial trial functions are used within each node and spatial Lagrange multipliers are used along the node boundaries. The internal angular approximation utilizes a complete odd-order set of spherical harmonics. Along the nodal boundaries, even and odd-order Rumyantsev interface conditions are combined with the spatial Lagrange multipliers to couple the nodes together. The new method is implemented in Cartesian x-y geometry and used to solve a fixed source benchmark problem.

KEYWORDS: neutron transport, nodal method, spherical harmonics, first-order form, VARIANT, void node problems

1. Introduction

The variational nodal method implemented in VARIANT [1,2] cannot be applied directly to voided nodes because of the cross section appearing in the denominator of the second-order even-parity equation. Problems are also encountered when very low-density media occupy a node. A potential alternative for these situations is to form the nodal response matrix using the first-order form of the transport equation, for then the cross section no longer appears in the denominator.

In this work a weighted residual approach is applied to the first-order form of the transport equation assuming the presence of isotropic scattering as well as an isotropic source. To maintain consistency, the same spatial trial functions used in VARIANT are applied both within the node and along the interfaces. Similarly, spherical harmonic approximations are applied to the angular variables. The result is an approximation for the angular flux within the node in terms of the group source and the neutron flux incident on the nodal surface. Given the nodal angular flux solution, the boundary angular flux distribution can be expressed in terms of the interface variables used in VARIANT. This is necessary if first- and second-order methods are to be used in conjunction with one another, which is the underlying goal of this work.

The response matrix formulation was implemented in MATHCAD [3] to examine the properties of the response matrix and apply them to model problems of limited problem size. The resulting response matrices were then imported into the VARIANT code where larger problems can be solved. The solutions obtained using the new method are promising and the method appears to be able to treat problems that have void regions.

2. Theory

The starting point for the new method is the first-order form of the transport equation with total and isotropic scattering cross sections σ and σ_s given by Eq. (1).

$$\hat{\Omega}\cdot\vec{\nabla}\psi(\vec{r},\hat{\Omega})+\sigma_t\psi(\vec{r},\hat{\Omega})-\sigma_s\phi(\vec{r})-s(\vec{r})=0, \qquad \vec{r}\in V, \qquad (1)$$

Using nodal decomposition of the spatial domain, we obtain the general boundary condition for each node where $\hat{n}$ is the outward normal.

$$\psi(\vec{r},\hat{\Omega})-\psi_\lambda(\vec{r},\hat{\Omega})=0, \qquad \vec{r}\in\Gamma,\ \hat{n}\cdot\hat{\Omega}<0 \quad (2)$$

These equations are multiplied by the weight vector $\mathbf{f}(\vec{r})$ and integrated over the nodal spatial domain to obtain the weighted residuals where bold faced lower and upper case symbols indicate column vectors and matrices, respectively.

$$\int dV\,\mathbf{f}\left[\hat{\Omega}\cdot\vec{\nabla}\psi+\sigma_t\psi-\sigma_s\phi-s\right]-\int_{\hat{\Omega}\cdot\hat{n}<0} d\Gamma\,\hat{\Omega}\cdot\hat{n}\mathbf{f}\left[\psi-\psi_\lambda\right]=0 \qquad (3)$$

Applying the divergence theorem to the streaming term and substituting the result into Eq. (3) yields

$$-\int dV\ \hat{\Omega}\cdot\vec{\nabla}\mathbf{f}\psi+\int dV\,\mathbf{f}\left[\sigma_t\psi-\sigma_s\phi-s\right]+\int_{\hat{\Omega}\cdot n>0} d\Gamma\,\hat{\Omega}\cdot\hat{n}\mathbf{f}\psi+\int_{\hat{\Omega}\cdot n<0} d\Gamma\,\hat{\Omega}\cdot\hat{n}\mathbf{f}\psi_\lambda=0. \qquad (4)$$

The general convex surface Γ is replaced by a sum of flat surfaces Γ_γ each with an outward normal $\hat{n}_\gamma$ such that each node is consistent with that defined in the VARIANT code [2].

2.1 Spatial Discretization

The spatial component of the angular flux is approximated within the node by

$$\psi(\vec{r},\hat{\Omega})=\mathbf{f}^T(\vec{r})\boldsymbol{\psi}(\hat{\Omega}), \qquad \vec{r}\in V \qquad (5)$$

$$\phi(\vec{r})=\mathbf{f}^T(\vec{r})\int d\Omega\,\boldsymbol{\psi}(\hat{\Omega})=\mathbf{f}^T(\vec{r})\boldsymbol{\psi}_o, \qquad \vec{r}\in V \qquad (6)$$

and the boundary condition by

$$\psi_\lambda(\vec{r},\hat{\Omega})=\mathbf{h}_\gamma^T(\vec{r})\boldsymbol{\psi}_{\lambda\gamma}(\hat{\Omega}), \qquad \vec{r}\in\Gamma_\gamma,\ \hat{n}_\gamma\cdot\hat{\Omega}<0 \qquad (7)$$

Inserting these approximations into Eq. (4) yields

$$\left[-\hat{\Omega}\cdot\int dV(\vec{\nabla}\mathbf{f})\mathbf{f}^T+\int dV\sigma_t\mathbf{f}\mathbf{f}^T+\sum_{\hat{\Omega}\cdot\hat{n}_\gamma>0}\hat{\Omega}\cdot\hat{n}_\gamma\int_\gamma d\Gamma\,\mathbf{f}\mathbf{f}^T\right]\boldsymbol{\psi}(\hat{\Omega})$$
$$=\int dV\sigma_s\mathbf{f}\mathbf{f}^T\int d\Omega'\,\boldsymbol{\psi}(\hat{\Omega}')+\mathbf{s}-\sum_{\hat{\Omega}\cdot\hat{n}_\gamma<0}\hat{\Omega}\cdot\hat{n}_\gamma\int_\gamma d\Gamma\,\mathbf{f}\,\mathbf{h}_\gamma^T\boldsymbol{\psi}_{\lambda\gamma}(\hat{\Omega}), \qquad (8)$$

and

$$\mathbf{s}=\int dV\,\mathbf{f}\,s. \qquad (9)$$

These equations can be compacted to obtain Eq. (10), by defining the integrals of the spatial trial functions as matrices and writing $\hat{\Omega}\cdot\int dV(\vec{\nabla}\mathbf{f})\mathbf{f}^T$ in terms of the direction cosines of $\hat{\Omega}$.

$$\left[-\sum_k\Omega_k\mathbf{U}_k+\mathbf{F}_t+\sum_{\hat{\Omega}\cdot\hat{n}_\gamma>0}\hat{\Omega}\cdot\hat{n}_\gamma\mathbf{W}_\gamma\right]\boldsymbol{\psi}(\hat{\Omega})=\mathbf{F}_s\int d\Omega'\,\boldsymbol{\psi}(\hat{\Omega}')+\mathbf{s}-\sum_{\hat{\Omega}\cdot\hat{n}_\gamma<0}\hat{\Omega}\cdot\hat{n}_\gamma\mathbf{D}_\gamma\boldsymbol{\psi}_{\lambda\gamma}(\hat{\Omega}) \qquad (10)$$

2.2 Spherical Harmonics Approximation

Next, $\mathbf{y}(\hat{\Omega})$, a vector of orthonormal spherical harmonics of order N, is used to approximate the angular component of the angular flux. The expansion takes the form

$$\psi(\hat{\Omega}) = \mathbf{y}^T(\hat{\Omega}) \otimes \mathbf{I}_s \boldsymbol{\Psi}, \tag{11}$$

The identity matrices $\mathbf{I}_s$ and $\mathbf{I}_\Omega$ have the dimensions of $\mathbf{f}$ and $\mathbf{y}$, respectively, and together they form the identity, $\mathbf{I} = \mathbf{I}_s \otimes \mathbf{I}_\Omega$. $\boldsymbol{\Psi}$ is a vector of unknown coefficients for the angular flux expansion which can be written as

$$\boldsymbol{\Psi} = \int d\Omega \left(\mathbf{y}(\hat{\Omega}) \otimes \mathbf{I}_s \right) \psi(\hat{\Omega}). \tag{12}$$

Once $\boldsymbol{\Psi}$ has been determined, the angular flux may be constructed within the node by combining Eqs. (5) and (11) to obtain

$$\psi(\vec{r}, \hat{\Omega}) = \mathbf{y}^T(\hat{\Omega}) \otimes \mathbf{f}^T(\vec{r}) \boldsymbol{\Psi}. \tag{13}$$

Inserting Eq. (11) into Eq. (10), weighting it with the vector $\mathbf{y}(\hat{\Omega}) \otimes \mathbf{I}_s$, and integrating over angle we obtain Eq. (14).

$$\left[-\sum_k \int d\Omega\, \Omega_k \mathbf{y}\mathbf{y}^T \otimes \mathbf{U}_k + \mathbf{I}_\Omega \otimes \mathbf{F}_t + \sum_\gamma \int_{\hat{\Omega}\cdot\hat{n}_\gamma > 0} d\Omega\, \hat{\Omega}\cdot\hat{n}_\gamma \mathbf{y}\mathbf{y}^T \otimes \mathbf{W}_\gamma - \int d\Omega\, \mathbf{y} \int d\Omega' \mathbf{y}^T \otimes \mathbf{F}_s \right] \boldsymbol{\Psi} \tag{14}$$
$$= \int d\Omega\, \mathbf{y} \otimes \mathbf{s} - \sum_\gamma \int_{\hat{\Omega}\cdot\hat{n}_\gamma < 0} d\Omega\, \hat{\Omega}\cdot\hat{n}_\gamma \mathbf{y} \otimes \mathbf{D}_\gamma \boldsymbol{\psi}_{\lambda\gamma}$$

Eq. (14) can be rewritten in the matrix form

$$\mathbf{A}\boldsymbol{\Psi} = \mathbf{J} \otimes \mathbf{s} - \sum_\gamma \int_{\hat{\Omega}\cdot\hat{n}_\gamma < 0} d\Omega\, \hat{\Omega}\cdot\hat{n}_\gamma \mathbf{y}(\hat{\Omega}) \otimes \mathbf{D}_\gamma \boldsymbol{\psi}_{\lambda\gamma}(\hat{\Omega}). \tag{15}$$

Inverting $\mathbf{A}$ and solving for $\boldsymbol{\Psi}$ yields

$$\boldsymbol{\Psi} = \mathbf{q} - \sum_\gamma \mathbf{A}^{-1} \int_{\hat{\Omega}\cdot\hat{n}_\gamma < 0} d\Omega\, \hat{\Omega}\cdot\hat{n}_\gamma \mathbf{y}(\hat{\Omega}) \otimes \mathbf{D}_\gamma \boldsymbol{\psi}_{\lambda\gamma}(\hat{\Omega}). \tag{16}$$

The angular flux within the node can be reconstructed using Eq. (13).

2.3 Interface Conditions

Next, $\boldsymbol{\psi}_{\lambda\gamma}(\hat{\Omega})$, the vector of spatial moments of the angular flux on the node surface, must be related to the even- and odd-parity space-angle moments employed in VARIANT. In VARIANT, even- and odd-parity spherical harmonics expansions are used to represent the angular flux distribution within the node volume and on its surface, respectively. These expansions can be combined to express the space-angle distribution of the flux at the nodal surface as

$$\psi(\vec{r}, \hat{\Omega}) = \mathbf{y}_+^T(\hat{\Omega}) \otimes \mathbf{f}^T(\vec{r}) \boldsymbol{\xi} + \mathbf{y}_-^T(\hat{\Omega}) \mathbf{K}_\gamma \boldsymbol{\Lambda} \otimes \mathbf{h}^T(\vec{r}) \boldsymbol{\chi}_\gamma, \qquad \vec{r} \in \Gamma_\gamma. \tag{17}$$

Here, $\mathbf{f}(\vec{r})$ and $\mathbf{h}(\vec{r})$ are the same vectors of continuous trial functions defined for $\vec{r} \in V$ and $\vec{r} \in \Gamma$, respectively. $\mathbf{y}_+(\hat{\Omega})$ and $\mathbf{y}_-(\hat{\Omega})$ are vectors of the even- and odd-parity spherical harmonics.

In VARIANT, the odd-parity spherical harmonics are rotated to align the polar angle with the outgoing normal. This allows the boundary condition implementations to be the same on all

surfaces. The square matrix $\mathbf{K}_\gamma$ is defined to represent the rotation from $\hat{n}_\gamma$ to the reference direction $\hat{n}_o$ as shown in Eq. (19).

$$\mathbf{y}_-(\hat{\Omega}) = \mathbf{K}_\gamma \mathbf{y}_{\gamma-}(\hat{\Omega}) \tag{18}$$

$$\mathbf{K}_\gamma = \int d\Omega\, \mathbf{y}_-(\hat{\Omega})\mathbf{y}_{\gamma-}^T(\hat{\Omega}) \tag{19}$$

At this point we define the $\mathbf{\Lambda}$ matrix, which extracts the necessary linear combinations of the odd-parity flux moments that must be held continuous across the nodal interfaces. In VARIANT, two sets of angular interface functions, and thus two $\mathbf{\Lambda}$, have been defined: the LI (linearly independent) set [4] and the Rumyantsev set [5].

The hybrid nodal method, upon which VARIANT is based, requires both $\boldsymbol{\chi}_\gamma$ and $\boldsymbol{\varphi}_\gamma$ to be continuous across nodal interfaces, where $\boldsymbol{\varphi}_\gamma$ is given by Eqs. (20) and (21).

$$\boldsymbol{\varphi}_\gamma = \mathbf{\Lambda}^T \mathbf{K}_\gamma^T \mathbf{E}_\gamma^T \otimes \mathbf{D}_\gamma^T \boldsymbol{\xi} \tag{20}$$

$$\mathbf{E}_\gamma = \int d\Omega\, \hat{\Omega}\cdot\hat{n}_\gamma \mathbf{y}_+(\hat{\Omega})\mathbf{y}_-^T(\hat{\Omega}) \tag{21}$$

The boundary flux $\boldsymbol{\psi}_{\lambda\gamma}(\hat{\Omega})$ in Eq. (16) can be expressed in terms of $\boldsymbol{\varphi}_\gamma$ and $\boldsymbol{\chi}_\gamma$ as shown in Eq. (22).

$$\boldsymbol{\psi}_{\lambda\gamma}(\hat{\Omega}) = \mathbf{y}_+^T(\hat{\Omega})(\mathbf{\Lambda}^T\mathbf{K}_\gamma^T\mathbf{E}_\gamma^T)^{-1} \otimes \mathbf{I}_\gamma \boldsymbol{\varphi}_\gamma + \mathbf{y}_-^T(\hat{\Omega})\mathbf{K}_\gamma\mathbf{\Lambda} \otimes \mathbf{I}_\gamma \boldsymbol{\chi}_\gamma \qquad \hat{n}_\gamma\cdot\hat{\Omega} < 0 \tag{22}$$

Eq. (22) can be multiplied by $\mathbf{D}_\gamma$ and the properties of $\otimes$ used to obtain

$$\mathbf{D}_\gamma\boldsymbol{\psi}_{\lambda\gamma}(\hat{\Omega}) = \mathbf{y}_+^T(\hat{\Omega})(\mathbf{\Lambda}^T\mathbf{K}_\gamma^T\mathbf{E}_\gamma^T)^{-1} \otimes \mathbf{D}_\gamma\boldsymbol{\varphi}_\gamma + \mathbf{y}_-^T(\hat{\Omega})\mathbf{K}_\gamma\mathbf{\Lambda} \otimes \mathbf{D}_\gamma\boldsymbol{\chi}_\gamma\,. \tag{23}$$

Finally, Eq. (23) is substituted into Eq. (16) resulting in

$$\mathbf{\Psi} = \mathbf{q} - \sum_\gamma \left[\mathbf{M}_\gamma^+(\mathbf{\Lambda}^T\mathbf{K}_\gamma^T\mathbf{E}_\gamma^T)^{-1} \otimes \mathbf{D}_\gamma\boldsymbol{\varphi}_\gamma + \mathbf{M}_\gamma^-\mathbf{K}_\gamma\mathbf{\Lambda} \otimes \mathbf{D}_\gamma\boldsymbol{\chi}_\gamma\right], \tag{24}$$

where

$$\mathbf{M}_\gamma^\pm = \mathbf{A}^{-1} \int\limits_{\hat{\Omega}\cdot\hat{n}_\gamma<0} d\Omega\, \hat{\Omega}\cdot\hat{n}_\gamma \mathbf{y}(\hat{\Omega}) \otimes \mathbf{I}_s \mathbf{y}_\pm^T(\hat{\Omega})\,. \tag{25}$$

2.4 Response Matrix Form

To obtain response matrices, continuity conditions must be imposed on the angular flux across the interfaces. Recall that the boundary condition given by Eq. (22), which specifies the angular distribution of the incoming flux (for $\hat{n}_\gamma\cdot\hat{\Omega} < 0$) in terms of $\boldsymbol{\varphi}_\gamma$ and $\boldsymbol{\chi}_\gamma$, is the approximation to Eq. (2).

The even- and odd-parity components can be treated separately, thereby obtaining Eqs. (26) and (27) where the matrices of Eq. (28) have been used.

$$\boldsymbol{\varphi}_\gamma = \mathbf{\Lambda}^T\mathbf{K}_\gamma^T\mathbf{E}_\gamma^T\Xi_+ \otimes \mathbf{D}_\gamma^T\mathbf{\Psi} \tag{26}$$

$$\boldsymbol{\chi}_\gamma = \left(\mathbf{\Lambda}^T\mathbf{\Lambda}\right)^{-1}\mathbf{\Lambda}^T\mathbf{K}_\gamma^T\Xi_- \otimes \mathbf{D}_\gamma^T\mathbf{\Psi} \tag{27}$$

$$\Xi_\pm = \int d\Omega\; \mathbf{y}_\pm(\hat{\Omega})\mathbf{y}^T(\hat{\Omega}) \tag{28}$$

Continuity can be imposed on Eq. (26), Eq. (27), or a linear combination of the two. Using weights of ½ a and *b*, which are free parameters, Eqs. (26) and (27) can be linearly combined as shown in Eqs. (29) and (30).

$$\tfrac{1}{2} a\boldsymbol{\varphi}_\gamma + b\boldsymbol{\chi}_\gamma = \boldsymbol{\Pi}_\gamma \boldsymbol{\Psi} \tag{29}$$

$$\boldsymbol{\Pi}_\gamma = \left[\tfrac{1}{2} a\boldsymbol{\Lambda}^T \mathbf{K}_\gamma^T \mathbf{E}_\gamma^T \boldsymbol{\Xi}_+ + b\left(\boldsymbol{\Lambda}^T \boldsymbol{\Lambda}\right)^{-1} \boldsymbol{\Lambda}^T \mathbf{K}_\gamma^T \boldsymbol{\Xi}_- \right] \otimes \mathbf{D}_\gamma^T \tag{30}$$

Combining Eqs. (24) and (30), Eq. (31) is obtained.

$$\tfrac{1}{2} a\boldsymbol{\varphi}_\gamma + b\boldsymbol{\chi}_\gamma = \boldsymbol{\Pi}_\gamma \mathbf{q} - \sum_{\gamma'} \boldsymbol{\Pi}_\gamma \mathbf{M}_{\gamma'}^+ (\boldsymbol{\Lambda}^T \mathbf{K}_{\gamma'}^T \mathbf{E}_{\gamma'}^T)^{-1} \otimes \mathbf{D}_{\gamma'} \boldsymbol{\varphi}_{\gamma'} - \sum_{\gamma'} \boldsymbol{\Pi}_\gamma \mathbf{M}_{\gamma'}^- \mathbf{K}_{\gamma'} \boldsymbol{\Lambda} \otimes \mathbf{D}_{\gamma'} \boldsymbol{\chi}_{\gamma'} \tag{31}$$

The variable transformation implemented in VARIANT, shown here as Eq. (32), can now be implemented in Eq. (31) to yield

$$\mathbf{j}^\pm = \tfrac{1}{4}\boldsymbol{\varphi} \pm \tfrac{1}{2}\boldsymbol{\chi} \tag{32}$$

$$(a+b)\mathbf{j}^+ + (a-b)\mathbf{j}^- = \boldsymbol{\Pi}\mathbf{q} - \mathbf{G}^+\mathbf{j}^+ - \mathbf{G}^-\mathbf{j}^-, \tag{33}$$

where the $\mathbf{G}_{\gamma\gamma'}^\pm$ matrices are given by Eq. (34).

$$\mathbf{G}_{\gamma\gamma'}^\pm = 2\boldsymbol{\Pi}_\gamma \mathbf{M}_{\gamma'}^+ (\boldsymbol{\Lambda}^T \mathbf{K}_{\gamma'}^T \mathbf{E}_{\gamma'}^T)^{-1} \otimes \mathbf{D}_{\gamma'} \pm \boldsymbol{\Pi}_\gamma \mathbf{M}_{\gamma'}^- \mathbf{K}_{\gamma'} \boldsymbol{\Lambda} \otimes \mathbf{D}_{\gamma'} \tag{34}$$

Solving for $\mathbf{j}^+$, the familiar response matrix equation given by Eq. (34) results, where the new matrices are defined in Eqs. (36) and (37).

$$\mathbf{j}^+ = \mathbf{R}\,\mathbf{j}^- + \mathbf{B}\mathbf{s} \tag{35}$$

$$\mathbf{R} = \left[(a+b)\mathbf{I} + \mathbf{G}^+\right]^{-1} \left[(b-a)\mathbf{I} - \mathbf{G}^-\right] \tag{36}$$

$$\mathbf{B} = \left[(a+b)\mathbf{I} + \mathbf{G}^+\right]^{-1} \boldsymbol{\Pi}\mathbf{A}^{-1}\mathbf{J} \otimes \mathbf{I}_s \tag{37}$$

The following section gives a brief discussion of some numerical results obtained for two benchmarks using the above method.

3. Modified Watanabe-Maynard

As stated earlier, the above matrix relationships have been implemented in MATHCAD and tested for stability and accuracy. In all of these tests, the first-order spherical harmonics method conserved neutrons and performed well. The response matrix formulation has been implemented in MATHCAD first because the angular matrices are far more difficult to implement in the existing VARIANT coding than in MATHCAD. The outer iteration solver in MATHCAD, however, can only solve problems of limited size (~50 nodes and low order approximations). To overcome this limitation, a patch was made for the VARIANT code, called VARIANT-F, so that VARIANT would perform the outer iterations using the response matrices obtained in MATHCAD.

The spherical harmonics method developed in Section 2 requires a complete odd-order expansion of spherical harmonics within the nodal domain. Along the interface we are free to use even- or odd-order sets of angular trial functions that obey Rumyantsev interface conditions [5] or the LI conditions [4]. As for the free parameters a and b, no theoretical justification has yet been established which would indicate optimum values. As a result, four different values of the free parameters a and b were considered. Our numerical studies have indicated that only the bounded $\boldsymbol{\varphi}_\gamma$ conditions (a = 2.0, b = 0.0) combined with a Rumyantsev interface trial function set yields acceptable solutions. The LI trial function set was eliminated because it did not result in solutions with asymptotic convergence towards the reference solution.

Several fixed-source, two-dimensional benchmark problems were used to test the new formulation. A simplification of a Watanabe-Maynard benchmark [6-7], shown in Fig. 1, displayed the largest errors and is discussed here. This benchmark was primarily used to assess the accuracy of the void treatment for the first-order formulation. The original benchmark defined a larger source region (shaded region) and smaller source magnitude than that shown in Fig. 1. The benchmark dimensions were simplified for this work to reduce the computational burden in MATHCAD.

The average flux within each node was used to assess the accuracy of the method rather than relying upon a rigorous reconstruction of the flux. All four flux traverses shown on the right hand side of Fig. 1 were investigated, but only a subset is presented here. The reference solution was obtained using the collision probability code DRAGON [6]. For perspective, discrete ordinate solutions were obtained using TWODANT [8].

Figure 2 gives the void flux traverse solutions for VARIANT-F using odd-order Rumyantsev interface conditions. Also included is a TWODANT S_{12} solution for comparison purposes. In general, the low order P_N solutions are very inaccurate near the source region and in the void region. However, the VARIANT-F solutions do eventually take up the shape of the reference DRAGON solution as the angular order is refined, but the accuracy is not very good. The TWODANT solutions display a little different behavior than the VARIANT-F solution. Near the source, the TWODANT solutions are very accurate, but in the void region and along the vacuum boundary (not shown), the ray effects lead to non physical characteristics.

The void flux traverse solutions for VARIANT-F using even-order Rumyantsev interface conditions are given in Fig. 3. Similar to the odd P_N solutions, the low order approximations are rather inaccurate near the source and void region. As the angular order is refined, clearly the VARIANT-F solutions tend to match the reference DRAGON solution.

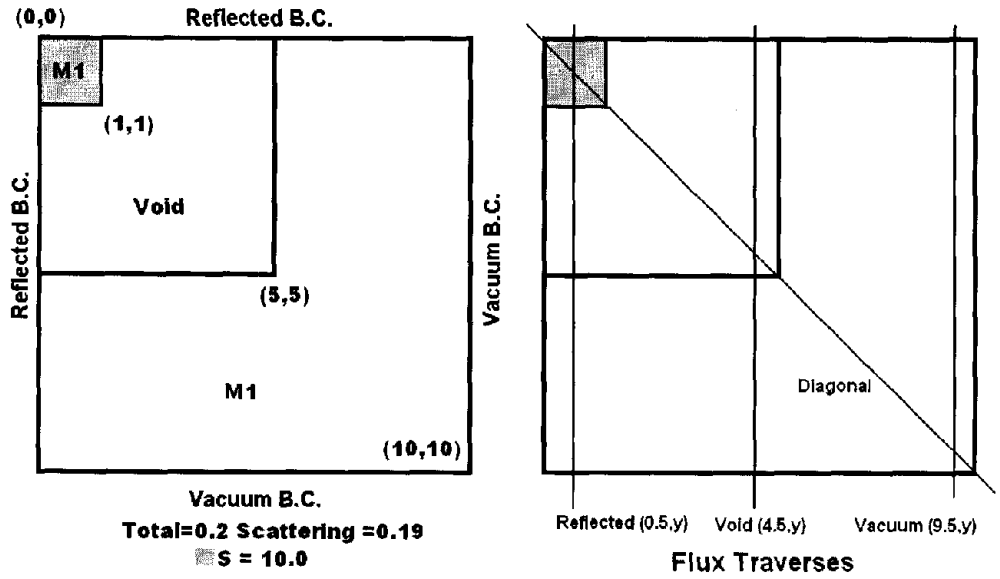

Fig. 1. Modified Watanabe-Maynard Benchmark Geometry

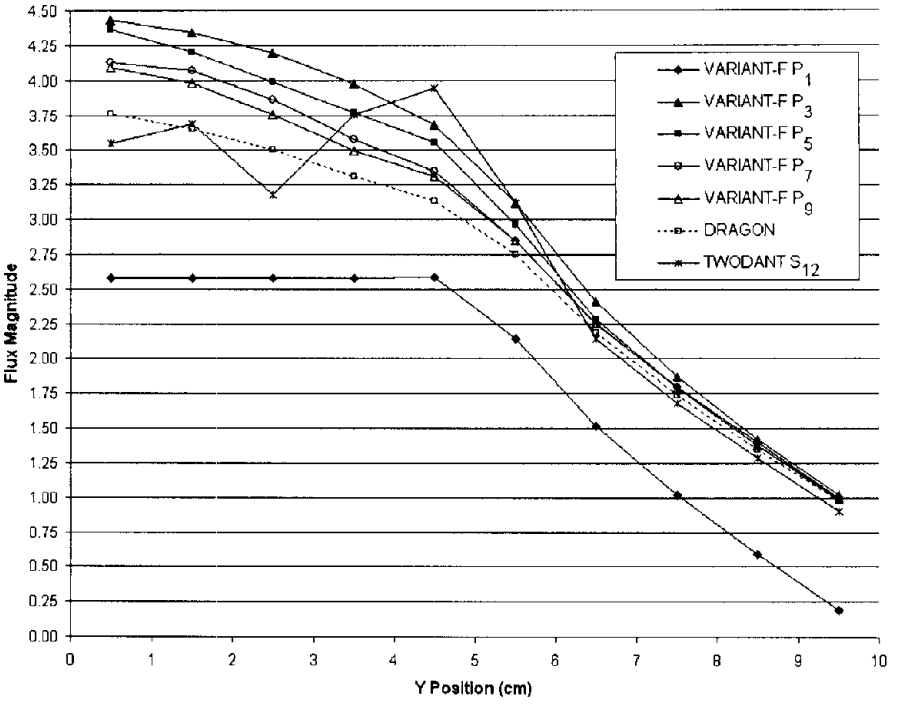

Fig. 2. Odd-order VARIANT-F Solutions to the Watanabe-Maynard Benchmark

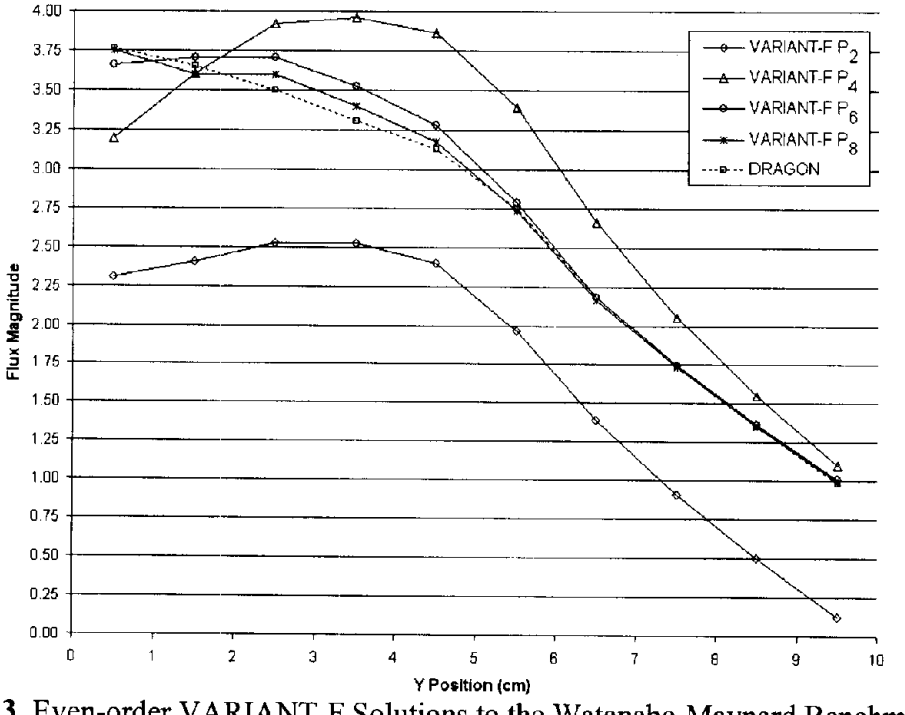

Fig. 3. Even-order VARIANT-F Solutions to the Watanabe-Maynard Benchmark

It is important to note that only some of the odd-order VARIANT-F solutions succeeded in reaching the desired convergence of 10^{-6} on the flux while in some cases the outer iteration procedure was stopped when the convergence error was less than 10^{-4}. The spectral radius of the lower order odd P_N problems was computed to be near 1.0 which makes the solution of the system of equations difficult at best. As the angular order is increased the spectral radius does improve and a converged solution (10^{-6}) was possible using P_9. Unlike the odd-order VARIANT-F solutions, there were no significant convergence problems with the even-order VARIANT-F solutions. Only a slight degradation in the spectral radius was observed as the angular order was increased.

At this point we can address the problem with the odd-order VARIANT-F solutions. In Section 2, we stated that an odd-order spherical harmonics approximation within the domain, or in Eq. (15), is necessary for the inversion in Eq. (16) regardless of the interface approximation. For the preceding odd-order VARIANT-F solutions we have assumed that the internal odd-order matched that of the order applied along the boundary. For the even-order VARIANT-F solutions the internal odd-order approximation clearly had to be greater than the even-order (P_2 on the boundary requires P_3 inside). The fundamental problem with the odd-order method is first seen in Eq. (17) or its discretized form, Eq. (22).

In Eq. (22), we are linking the incoming neutron flux entering the nodal domain to a set of spherical harmonic functions which are continuous across the nodal interface. The underlying subtlety is that the use of continuous angular trial functions actually defines both the incoming and outgoing angular distribution of neutrons along the boundary. For odd-order VARIANT-F solutions this amounts to over-constraining the angular dependence of the flux since the angular order within the domain is the same as that along the boundary. We can draw parallels to the spatial domain to further explain this. Assuming we used a 6^{th} order polynomial expansion of the flux (spatial) within the domain, we obviously cannot employ a 6^{th} order spatial approximation to the flux along the boundary since the resulting system of equations would be rank deficient.

The success of the even-order approximation comes from the fact that it bounds the magnitude of key higher order angular terms but does not explicitly bound all of the terms on each surface. Additional work has been initiated to determine the proper odd-order boundary conditions which would be compatible with the VARIANT code and not lead to the preceding accuracy and convergence problems. These conditions would obviously have odd-order interface conditions that are of lower order than that used internal to the node (P_1 along the boundary using P_3 inside, etc...). At this point the P_1 conditions have generally been found to be convergent using any higher order angular approximation within the nodal domain.

4. Conclusions

For the Watanabe-Maynard benchmark, the first-order form using odd-order interface conditions had substantial inaccuracies and displayed significant convergence problems attributed to an over-constrained angular flux. With even-order interface conditions, there was still significant error, but no convergence problems were present.

In general, the solutions obtained using VARIANT-F proved to have the correct flux shape, but an insufficient space-angle approximation and slow convergence in the outer iterations prevented it from obtaining accurate solutions. Overall the new method does appear to be able to treat void regions although a higher order angular approximation is clearly necessary for problems containing voids. From a researcher's viewpoint, it is quite gratifying to be able to

demonstrate a method capable of treating void regions that is based explicitly on the spherical harmonics method. To our knowledge, this is the first time this has been achieved. Most importantly, the new formulation is compatible with the existing second-order method available in the VARIANT code.

As a final note, additional research has shown that a nodal first-order integral method compatible with a recent second-order integral method [9] can also treat void problems. This integral method is computationally more efficient and generally more accurate (with respect to angular order) than the preceding first-order spherical harmonics method.

Acknowledgements

This work was supported by the U.S. Department of Energy under Contract numbers DE-FG07-01ID1410 and W-31-109-Eng-38.

References

1) C. B. Carrico, E.E. Lewis and G. Palmiotti, "Three Dimensional Variational Nodal Transport Methods for Cartesian, Triangular and Hexagonal Criticality Calculations," Nucl. Sci. Eng. 111, 168 (1992).
2) G. Palmiotti, E. E. Lewis & C. B. Carrico, "VARIANT: VARIational Anisotropic Nodal Transport for Multidimensional Cartesian and Hexagonal Geometry Calculation," Argonne National Laboratory ANL-95/40, 1995.
3) Mathsoft, Mathcad 6.0 Professional Edition Users Manual. Mathsoft, 1995.
4) G. Palmiotti, C. B. Carrico, and E. E. Lewis, "Variational Nodal Transport Methods with Anisotropic Scattering," Nucl. Sci. Eng. 115, 233-234 (1993).
5) W. S. Yang, M. A. Smith, G. Palmiotti & E. E. Lewis, "Interface Conditions and Angular Trial Functions in Variational Nodal Formulation for Multi-dimensional Spherical Harmonics Method," to be submitted to Nucl. Sci. Eng. (2003).
6) G. Marleau, A. Hébert & R. Roy, "A User's Guide for DRAGON," Ecole Polytechnique de Montréal, December 1997.
7) Y. Watanabe and C. W. Maynard, "The discrete cones method in two dimensional neutron transport computations," University of Wisconsin. Report UWFDM-574 (1984).
8) R. E. Alcouffe, F. W. Brinkley, D. R. Marr, and R. D. O'dell, "User's Guide for TWODANT: A Code Package for Two-Dimensional, Diffusion-Accelerated Neutral Particle Transport," LA-10049-M, Los Alamos National Laboratory (1984).
9) M. A. Smith, G. Palmiotti, E. E. Lewis & N. Tsoulfanidis, "An Integral Form of the Variational Nodal Method," to be published in Nucl. Sci. Eng. (2004).

Appendix E

To appear in *Ann. Nucl Energy*

Much Ado about Nothing: Response Matrices for Void Regions

E. E. Lewis
Department of Mechanical Engineering
Northwestern University
Evanston IL 60201 U.S.A.
e-lewis@northwestern.edu

Abstract

Weak form Galerkin approaches are examined for obtaining response matrices for void regions - that is regions where nothing is present. The need arises in spherical harmonics methods based on second-order forms of the neutron transport equation; the methods fail in voids because the cross section appearing in the equation's denominator then vanishes. The diffusion approximation, being the lowest-order spherical harmonic method, is first employed as a vehicle for examining response matrices derived from both primal and dual weak forms of the mixed-first-order and second-order transport equations. Those for which discretization results in singular matrix equations as the cross section goes to zero are rejected. First-order- mixed formulations with modified natural boundary conditions are shown to lead to nonsingular response matrices for voids. The primal method is chosen as the better of the two candidates for generalization from the diffusion to the transport equations, and the transport formulation is presented.

1. Introduction

Computational methods based on the second-order form of the transport equation have found wide spread use in nuclear calculations, the most widely used of these, of course, being the neutron diffusion equation. Spherical harmonics expansions in angle have been combined with spatial finite element to treat situations where higher-order angular approximations are needed, (deOliveira, 1986; Carrico, et. al. 1992; Lewis et. al. 1996). A shortcoming of second-order transport methods, however, stems from the cross section that appears in the denominator. The result is that the methods cannot be applied directly to void regions – that is to regions where nothing is present.

In particular, the void region problem appears in variational nodal methods, such as those contained in the widely-used VARIANT code (Palmiotti, et. al., 1995). These methods combine spherical harmonics expansions with hybrid finite elements to obtain solutions of the second-order transport equations in response matrix form. The challenge is thus to obtain void region response matrices that are compatible with spherical harmonics expansions and hybrid finite elements.

Recent work in applying spherical harmonics expansions to the first-order form of the transport equations has given rise to void-region response matrices that appear to be compatible with VARIANT, although a number of ambiguities remain (Smith, et. al, 2004). Concurrently, research on mixed primal and dual forms of the transport equation has shown that both even- and odd-order spherical harmonics expansions can be combined with hybrid finite elements to obtain solutions to benchmark problems, albeit not in response matrix form, and not where void regions are present (Van Criekingen, 2004; Van Criekingen, et. al. 2004). What follows draws on these two approaches to examine in some detail the application of primal and dual mixed methods to generate response matrices in the diffusion approximation. Both natural and modified natural boundary conditions are used to obtain response matrices of the T, T^1, and R classes in the taxonomy of Lindahl and Weiss (1981). An objective of this analysis is to determine which approached may offer the potential for creating response matrices for void regions. It is understood that in the diffusion or P_1 approximation any response matrix would be at best highly inaccurate, and would need to be generalized to higher-order angular approximations to be of any value in void regions. But by examining the methods in the diffusion approximation we can determine which approaches lead to singular matrices and abandon them, for if they are singular in the diffusion approximation they will remain so if higher-order spherical harmonics are employed.

In the following section the various forms of the mix-coupled and second-order diffusion equations are presented. In section 3, spatial discretization is employed to obtain response matrices. In section 4 the response matrices are examined in the limit as the cross section goes to zero, and the primal mixed form with modified natural boundary conditions is chosen as a candidate for generalization to higher-order space angle approximations. In section 5, the transport form of the primal mixed equations and the concomitant modified natural boundary conditions are presented. The final section contains a brief discussion.

2. Diffusion Formulations

We begin by writing the mixed-coupled diffusion (or P_1) equations over a volume V with surface Γ:

$$\vec{\nabla}\cdot\vec{J}(\vec{r})+\sigma_r\phi(\vec{r})=s(\vec{r}), \qquad \vec{r}\in V \qquad (1)$$

and

$$\vec{\nabla}\phi(\vec{r})+3\sigma\vec{J}(\vec{r})=0, \qquad \vec{r}\in V \qquad (2)$$

where ϕ and $\vec{J}$ are the scalar flux and current, and σ and σ_r are the macroscopic total and removal cross section. Our treatment is restricted of isotopic scattering and sources where the diffusion and P_1 approximations are identical. Either $\vec{J}$ or ϕ may be eliminated between these equations to obtain the second order even- or odd- parity forms of the equations respectively. We obtain the weak forms of mixed and second-order equations by first multiplying Eqs. (1) and (2) by weight functions and then integrating

over the volume of the problem domain. Let $\tilde{\phi}$ and $\tilde{\vec{J}}$ be a scalar and a vector weight function. Then multiplying Eq. (1) by $\tilde{\phi}$ and integrating over volume, we have

$$\int dV \tilde{\phi}(\vec{\nabla}\cdot\vec{J}+\sigma_r\phi-s)=0. \tag{3}$$

Likewise, weighting Eq. (2) with $\tilde{\vec{J}}$ and integrated over the volume yields

$$\int dV \tilde{\vec{J}}\cdot(\vec{\nabla}\phi+3\sigma\vec{J})=0. \tag{4}$$

2.1 Primal Equations

We obtain the primal equations by applying the divergence theorem to the first term of Eq. (3):

$$\int dV\left[-(\vec{\nabla}\tilde{\phi})\cdot\vec{J}+\tilde{\phi}(\sigma_r\phi-s)\right]+\int d\Gamma\tilde{\phi}\hat{n}\cdot\vec{J}=0. \tag{5}$$

If we use Eq. (2) to eliminate the current from this equation we obtain the primal weak form of the second-order diffusion approximation:

$$\int dV\left[(3\sigma)^{-1}(\vec{\nabla}\tilde{\phi})\cdot\vec{\nabla}\phi+\tilde{\phi}(\sigma_r\phi-s)\right]+\int d\Gamma\tilde{\phi}\hat{n}\cdot\vec{J}=0. \tag{6}$$

In the primal form, flux continuity across interfaces is enforced by

$$\int d\Gamma\hat{n}\cdot\tilde{\vec{J}}(\phi-\phi')=0, \tag{7}$$

where ϕ and ϕ' indicate flux values on opposite sides of the interface, where $\hat{n}'=-\hat{n}$. Equations (5), (4) and (7) constitute the primal weak form of the coupled first-order equations. Equations (6) and (7) constitute the corresponding second order form.

2.2 Dual Equations

The dual forms are obtained by applying the divergence theorem to Eq. (4):

$$\int dV\left[-(\vec{\nabla}\cdot\tilde{\vec{J}})\phi+3\sigma\tilde{\vec{J}}\cdot\vec{J}\right]+\int d\Gamma\hat{n}\cdot\tilde{\vec{J}}\phi=0. \tag{8}$$

The second-dual form then results from utilizing Eq. (1) to eliminate ϕ from this expression:

$$\int dV\left[\sigma_r^{-1}(\vec{\nabla}\cdot\tilde{\vec{J}})\vec{\nabla}\cdot\vec{J}+3\sigma\tilde{\vec{J}}\cdot\vec{J}-\sigma_r^{-1}(\vec{\nabla}\cdot\tilde{\vec{J}})s\right]+\int d\Gamma\hat{n}\cdot\tilde{\vec{J}}\phi=0. \tag{9}$$

The dual continuity condition is

$$\int d\Gamma\tilde{\phi}\,\hat{n}\cdot(\vec{J}-\vec{J}')=0, \tag{10}$$

where $\vec{J}$ and $\vec{J}'$ indicate current values on opposite sides of the interface.

If we were to present the foregoing equations in variational form $\tilde{\vec{J}}$ and $\tilde{\phi}$ would appear as Lagrange multipliers at the interfaces for primal and dual methods respectively, and continuity conditions of Eqs (7) and (10) would result from requiring the functions to be stationary with respect to variations in the Lagrange multipliers. Employing weighted residuals we may thus determine ϕ at the boundaries, given $\vec{J}\cdot\hat{n}$ at the boundary in the primal formulation or conversely $\vec{J}\cdot\hat{n}$ at the boundary given ϕ at the boundaries with the dual method. We can thus obtain what Lindahl and Weiss(1981) classified as T^{-1} and T response matrices respectively. They may then be converted to the standard R matrix form by changing variables from the flux and current to the partial current variables

$$J_n^+ = \tfrac{1}{4}\phi + \tfrac{1}{2}\hat{n}\cdot\vec{J} \tag{11}$$

and

$$J_n^- = \tfrac{1}{4}\phi - \tfrac{1}{2}\hat{n}\cdot\vec{J} \tag{12}$$

By modifying the natural boundary conditions we may also obtain the R matrix form directly, that is we may specify the incoming partial current J_n^- and determine the outgoing partial current J_n^+.

2.3 Modified Primal Equations

For the modified primal formulations, we begin by weighting Eq. (12) with $\tilde{\phi}$ and integrating over the domain surface:

$$\int d\Gamma\tilde{\phi}(\tfrac{1}{4}\phi - \tfrac{1}{2}\hat{n}\cdot\vec{J} - J_n^-) = 0 \tag{13}$$

we then add this expression to Eq. (5) or Eq. (6) to obtain the coupled or the second-order primal formulations with incoming partial current natural boundary conditions:

$$\int dV\left[-(\vec{\nabla}\tilde{\phi})\cdot\vec{J} + \tilde{\phi}(\sigma_r\phi - s)\right] + \int d\Gamma\tfrac{1}{2}\tilde{\phi}\phi - 2\int d\Gamma\tilde{\phi}J_n^- = 0 \tag{14}$$

$$\int dV\left[(3\sigma)^{-1}(\vec{\nabla}\tilde{\phi})\cdot\vec{\nabla}\phi + \tilde{\phi}(\sigma_r\phi - s)\right] + \int d\Gamma\tfrac{1}{2}\tilde{\phi}\phi - 2\int d\Gamma\tilde{\phi}J_n^- = 0 \tag{15}$$

where Eq. (4) remains unchanged in the coupled case. Corresponding to the continuity conditions for the unmodified primal methods, we must construct interface continuity conditions compatible with the modified interface conditions. Since at an interface $\hat{n}' = -\hat{n}$, we obtain from Eqs. (11) and (12), $J_n^+ = J_{n'}^-$. Thus for the primal methods with modified boundary conditions, we weight Eq. (11) with $\tilde{\phi}$ to obtain

$$\int d\Gamma\tilde{\phi}(\tfrac{1}{4}\phi + \tfrac{1}{2}\hat{n}\cdot\vec{J} - J_n^+) = 0\,. \tag{16}$$

2.4 Modified Dual Equations

For the modified dual formulations we multiply Eq. (12) by $\tilde{\vec{J}} \cdot \hat{n}$ to obtain

$$\int d\Gamma \hat{n} \cdot \tilde{\vec{J}} (¼\phi - ½ \hat{n} \cdot \vec{J} - J_n^-) = 0 . \tag{17}$$

Multiplying this expression by 4 and subtracting from Eqs. (8) or (9) then yields the mixed-coupled or the second-order forms of the dual method with modified natural boundary conditions

$$\int dV \left[-(\vec{\nabla} \cdot \tilde{\vec{J}})\phi + 3\sigma \tilde{\vec{J}} \cdot \vec{J} \right] + 2 \int d\Gamma \hat{n} \cdot \tilde{\vec{J}} \hat{n} \cdot \vec{J} + 4 \int d\Gamma \hat{n} \cdot \tilde{\vec{J}} J_n^- = 0 , \tag{18}$$

or

$$\int dV \left[\sigma_r^{-1} (\vec{\nabla} \cdot \tilde{\vec{J}}) \vec{\nabla} \cdot \vec{J} + 3\sigma \tilde{\vec{J}} \cdot \vec{J} - \sigma_r^{-1} (\vec{\nabla} \cdot \tilde{\vec{J}}) s \right] + 2 \int d\Gamma \hat{n} \cdot \tilde{\vec{J}} \hat{n} \cdot \vec{J} + 4 \int d\Gamma \hat{n} \cdot \tilde{\vec{J}} J_n^- = 0 . \tag{19}$$

where Eq. (3) remains the same in the coupled case. For the dual method with modified boundary conditions, we again note that $J_n^+ = J_n^-$. and weight Eq. (11) with $\hat{n} \cdot \tilde{\vec{J}}$ to obtain

$$\int d\Gamma \hat{n} \cdot \tilde{\vec{J}} (¼\phi + ½ \hat{n} \cdot \vec{J} - J_n^+) = 0 . \tag{20}$$

2.5 Summary of Equations

Before proceeding, It is useful to summarize the eight weak-form formulations that we have presented for the diffusion equation. The summary is presented as Table 1. The primal forms have Neumann natural boundary conditions. If the surface terms are eliminated these correspond to $\vec{J} \cdot \hat{n} = 0$. In the inhomogeneous form we are required to specify $\vec{J} \cdot \hat{n}$. Likewise, the dual forms have Dirichlet boundary conditions, corresponding to $\phi = 0$ when the surface term is eliminated. In both modified primal and dual formulations these are replaced by Robin conditions on the partial current $\vec{J}_n^-$. In primal methods trial functions for ϕ but not $\vec{J}$ must be continuous within V, since only flux derivatives appear. Conversely, in dual methods $\vec{J}$ but not ϕ trial functions must be continuous within V, since only current derivatives appear.

Since we are concerned with response matrix formulations that can treat void regions, we eliminate the second-order methods contained in Eqs. (15) and (18), since the total and removal cross-sections appear respectively in the denominators of the primal and dual second-order formulations.

3. Diffusion Response Matrices

To discretize the foregoing equations and obtain response matrices we employ Galerkin weighting. However we employ different sets of spatial expansion functions within the node for ϕ and $\vec{J}$ within the node, and a second set of trial functions for $\vec{J}\cdot\hat{n}$, ϕ and J_n^- on the interfaces for the primal, dual, and modified formulations respectively. The interface expansions are also employed for the weight functions in Eqs. (9) , (10), (19), and (20). For brevity we set the source term to zero, and limit our treatment to two-dimensions.

We begin by approximating the flux and current within V:

$$\phi(\vec{r}) \approx \mathbf{f}_+^T(\vec{r})\boldsymbol{\phi}, \qquad \vec{r} \in V \qquad (21)$$

and

$$\vec{J}(\vec{r}) \approx \vec{\mathbf{f}}_-^T(\vec{r})\mathbf{j}. \qquad \vec{r} \in V \qquad (22)$$

Here, $\mathbf{f}_+$ and $\vec{\mathbf{f}}_+$ are column vectors of known trial functions, and $\boldsymbol{\phi}$ and $\mathbf{j}$ are the unknown flux and current coefficients. More specifically,

$$\vec{\mathbf{f}}_-^T(\vec{r}) = \left[\hat{i}\,\mathbf{f}_x^T(\vec{r}),\ \ \hat{j}\,\mathbf{f}_y^T(\vec{r})\right], \qquad (23)$$

and

$$\mathbf{j}^T = \left[\mathbf{j}_x^T, \mathbf{j}_y^T\right]. \qquad (24)$$

The vectors $\mathbf{f}_+, \mathbf{f}_x$, and $\mathbf{f}_y$ are assumed to be polynomial trial functions that are orthonormal over V. For Galerkin weighting, the weight functions become $\tilde{\phi}(\vec{r}) \rightarrow \mathbf{f}_+(\vec{r})$ and, $\tilde{\vec{J}}(\vec{r}) \rightarrow \vec{\mathbf{f}}_-(\vec{r})$ for $\vec{r} \in V$.

We approximate the interface conditions as

$$\hat{n}\cdot\vec{J}(\vec{r}) \approx \mathbf{h}^T(\vec{r})\mathbf{j}_\Gamma \qquad \vec{r} \in \Gamma \qquad (25)$$

for the primal method and

$$\phi \approx \mathbf{h}^T(\vec{r})\boldsymbol{\phi}_\Gamma. \qquad \vec{r} \in \Gamma \qquad (26)$$

for the dual method. The vector $\mathbf{h}$ consists of orthonormal polynomial trial functions defined only on the interface; $\boldsymbol{\phi}_\Gamma$ and $\mathbf{j}_\Gamma$ are the unknown interface coefficients. For the modified primal and dual methods the interface approximation for the partial current is

$$J_n^-(\vec{r}) \approx \mathbf{h}^T(\vec{r})\mathbf{j}_\Gamma^-. \qquad \vec{r} \in \Gamma \qquad (27)$$

For consistent Galerkin weighting, we take the interface weight functions as $\hat{n}\cdot\tilde{\vec{J}}(\vec{r})\to\mathbf{h}(\vec{r})$, and $\tilde{\phi}(\vec{r})\to\mathbf{h}(\vec{r})$ for $\vec{r}\in\Gamma$.

Substituting these approximations and weight functions into the pairs of equations given in Table 1 for each of the coupled first-order forms, we obtain:

Primal:

$$\begin{bmatrix} -\sigma_r\mathbf{I} & \mathbf{B}_p \\ \mathbf{B}_p^T & 3\sigma\mathbf{I} \end{bmatrix}\begin{bmatrix} \boldsymbol{\phi} \\ \mathbf{j} \end{bmatrix} = -\begin{bmatrix} \mathbf{M}_p \\ \mathbf{0} \end{bmatrix}\mathbf{j}_\Gamma \tag{28A}$$

Modified Primal:

$$\begin{bmatrix} -\mathbf{W}_p-\sigma_r\mathbf{I} & \mathbf{B}_p \\ \mathbf{B}_p^T & 3\sigma\mathbf{I} \end{bmatrix}\begin{bmatrix} \boldsymbol{\phi} \\ \mathbf{j} \end{bmatrix} = \begin{bmatrix} -2\mathbf{M}_p \\ \mathbf{0} \end{bmatrix}\mathbf{j}_\Gamma^- \tag{28B}$$

Dual:

$$\begin{bmatrix} \sigma_r\mathbf{I} & \mathbf{B}_d \\ \mathbf{B}_d^T & -3\sigma\mathbf{I} \end{bmatrix}\begin{bmatrix} \boldsymbol{\phi} \\ \mathbf{j} \end{bmatrix} = -\begin{bmatrix} \mathbf{0} \\ \mathbf{M}_d \end{bmatrix}\boldsymbol{\phi}_\Gamma \tag{28C}$$

Modified Dual

$$\begin{bmatrix} \sigma_r\mathbf{I} & \mathbf{B}_d \\ \mathbf{B}_d^T & -\mathbf{W}_d-3\sigma\mathbf{I} \end{bmatrix}\begin{bmatrix} \boldsymbol{\phi} \\ \mathbf{j} \end{bmatrix} = \begin{bmatrix} \mathbf{0} \\ 4\mathbf{M}_d \end{bmatrix}\mathbf{j}_\Gamma^- \tag{28D}$$

The matrices are given by

$$\mathbf{B}_p = \int dV(\vec{\nabla}\mathbf{f}_+)\cdot\vec{\mathbf{f}}_-^T \qquad \mathbf{B}_d = \int dV\mathbf{f}_+\vec{\nabla}\cdot\vec{\mathbf{f}}_-^T$$

$$\mathbf{M}_p = \int d\Gamma\mathbf{f}_+\mathbf{h}^T \qquad \mathbf{M}_d = \int d\Gamma\hat{n}\cdot\vec{\mathbf{f}}_-\mathbf{h}^T$$

$$\mathbf{W}_p = \tfrac{1}{2}\int d\Gamma\mathbf{f}_+\mathbf{f}_+^T \qquad \mathbf{W}_d = 2\int d\Gamma\hat{n}\cdot\vec{\mathbf{f}}_-\hat{n}\cdot\vec{\mathbf{f}}_-^T$$

Likewise, the discretization results in the continuity conditions listed in Table 1 require continuity of the following interface moments:

Primal: $$\boldsymbol{\phi}_\Gamma = \mathbf{M}_p^T\boldsymbol{\phi}\,. \tag{29A}$$

Dual: $$\mathbf{j}_\Gamma = \mathbf{M}_d^T\mathbf{j} \tag{29B}$$

Modified (Primal or Dual) $$\mathbf{j}_\Gamma^+ = \tfrac{1}{4}\mathbf{M}_p^T\boldsymbol{\phi} + \tfrac{1}{2}\mathbf{M}_d^T\mathbf{j} \tag{29C}$$

We may combine Eqs. (28) and (29) to yield

Primal: $$\boldsymbol{\phi}_\Gamma = -\mathbf{K}_p \mathbf{j}_\Gamma \tag{30A}$$

Modified Primal: $$\mathbf{j}_\Gamma^+ = \mathbf{K}_{mp} \mathbf{j}_\Gamma^- \tag{30B}$$

Dual: $$\mathbf{j}_\Gamma = -\mathbf{K}_d \boldsymbol{\phi}_\Gamma \tag{30C}$$

Modified Dual: $$\mathbf{j}_\Gamma^+ = \mathbf{K}_{md} \mathbf{j}_\Gamma^- \tag{30D}$$

The matrices are defined by

$$\mathbf{K}_p = \begin{bmatrix} \mathbf{M}_p \\ \mathbf{0} \end{bmatrix}^T \begin{bmatrix} -\sigma_r \mathbf{I} & \mathbf{B}_p \\ \mathbf{B}_p^T & 3\sigma \mathbf{I} \end{bmatrix}^{-1} \begin{bmatrix} \mathbf{M}_p \\ \mathbf{0} \end{bmatrix} \qquad \mathbf{K}_{mp} = \begin{bmatrix} \tfrac{1}{2}\mathbf{M}_p \\ \tfrac{1}{4}\mathbf{M}_d \end{bmatrix}^T \begin{bmatrix} -\mathbf{W}_p - \sigma_r \mathbf{I} & \mathbf{B}_p \\ \mathbf{B}_p^T & 3\sigma \mathbf{I} \end{bmatrix}^{-1} \begin{bmatrix} -2\mathbf{M}_p \\ \mathbf{0} \end{bmatrix}$$

$$\mathbf{K}_d = \begin{bmatrix} \mathbf{0} \\ \mathbf{M}_d \end{bmatrix}^T \begin{bmatrix} \sigma_r \mathbf{I} & \mathbf{B}_d \\ \mathbf{B}_d^T & -3\sigma \mathbf{I} \end{bmatrix}^{-1} \begin{bmatrix} \mathbf{0} \\ \mathbf{M}_d \end{bmatrix} \qquad \mathbf{K}_{md} = \begin{bmatrix} \tfrac{1}{2}\mathbf{M}_p \\ \tfrac{1}{4}\mathbf{M}_d \end{bmatrix}^T \begin{bmatrix} \sigma_r \mathbf{I} & \mathbf{B}_d \\ \mathbf{B}_d^T & -\mathbf{W}_d - 3\sigma \mathbf{I} \end{bmatrix}^{-1} \begin{bmatrix} \mathbf{0} \\ 4\mathbf{M}_d \end{bmatrix}$$

The unmodified primal and dual formulations correspond respectively to the T^{-1} and T formulations in the taxonomy of Lindahl and Weiss (1981), whereas both the modified primal and modified dual methods are already in the standard R form:

$$\mathbf{j}_\Gamma^+ = \mathbf{R} \mathbf{j}_\Gamma^- . \tag{31}$$

The T and T^{-1} forms may be transformed to R form simply by letting

$$\mathbf{j}_\Gamma^\pm = \tfrac{1}{4}\boldsymbol{\phi}_\Gamma \pm \tfrac{1}{2}\mathbf{j}_\Gamma \tag{32}$$

to yield

$$\mathbf{R}_p = (\tfrac{1}{2}\mathbf{K}_p + \mathbf{I})^{-1}(\tfrac{1}{2}\mathbf{K}_p - \mathbf{I}), \tag{33}$$

and

$$\mathbf{R}_d = (\mathbf{I} + 2\mathbf{K}_d)^{-1}(\mathbf{I} - 2\mathbf{K}_d) . \tag{34}$$

4. Diffusion Response Matrices in Void Regions

For plane and x-y geometries the primal second-order method may be combined with the lowest order trial functions (i. e. with $\phi(\vec{r})$ quadratic in V and $\hat{n} \cdot \vec{J}(\vec{r})$ constant on each surface of Γ) to obtain analytic expressions for the response matrix (Lewis and Palmiotti, 1998). In the limit as $\sigma \to 0$, the cross section cancels between numerator and

denominator, yielding diffusion response matrices for void regions. In plane geometry the response matrix takes the form

$$\mathbf{R} = \begin{bmatrix} r & t \\ t & r \end{bmatrix} \tag{35}$$

and one obtains the expected values for the transmission and reflection of t=1.0 and r =0.0. In x-y geometry, where the response matrix for a square has the form

$$\mathbf{R} = \begin{bmatrix} r & d & t & d \\ d & r & d & t \\ t & d & r & d \\ d & t & d & r \end{bmatrix} \tag{36}$$

one obtains t=1/2, d=1/2 and r=-1/2. Thus while neutron conservation is maintained, a nonphysical value of −1/2 is obtained for the reflection. This is not surprising, since one cannot expect to treat void streaming accurately with the diffusion approximation. The possibility remains open for obtaining more accurate results with the use of higher-order space-angle approximations. Unfortunately, obtaining analytical solutions that then can be taken to the limit as $\sigma \to 0$ becomes an insurmountable hurdle. Thus for practical application we must rely on coupled methods, for which σ does not appear in the denominator. Examining Eqs. (28), however, we see that as $\sigma \to 0$ the diagonal blocks of the unmodified primal and dual methods vanish, yielding singular coefficient matrices. Thus we eliminate the unmodified methods from further consideration.

To proceed, we attempt to obtain void region response matrices using modified primal and dual methods. To accomplish this, restrictions must be applied to the polynomial orders of the trial function in order to avoid obtaining rank deficient coefficient matrices (Carrico, et. al., 1994; Van Criekingen, 2004). The interface trial function **h** must be of lower order than the interior trial functions. We take **h** to be piecewise constant with one unique value on each of the two or four surfaces of Γ. In the primal method, $\mathbf{f}_+$ must be one order higher than $\mathbf{f}_x$ and $\mathbf{f}_y$; conversely in the dual method the order of $\mathbf{f}_x$ and $\mathbf{f}_y$ must be higher than of $\mathbf{f}_+$. The following trial and weight functions meet these conditions:

One Dimension ($-1 \le x \le +1$)

Primal: $$\mathbf{f}_+^T = \left[1, \sqrt{3}x, (\sqrt{5}/2)(3x^2-1)\right],\ \mathbf{f}_x^T = \left[1, \sqrt{3}x\right] \tag{37}$$

Dual: $$\mathbf{f}_+^T = \left[1, \sqrt{3}x\right], \qquad \mathbf{f}_x^T = \left[1, \sqrt{3}x, (\sqrt{5}/2)(3x^2-1)\right] \tag{38}$$

Two dimensions ($-1 \le x \le +1$, $-1 \le y \le +1$)

Primal: $$\mathbf{f}_+^T = \left[1, \sqrt{3}x, \sqrt{3}y, (\sqrt{5}/2)(3x^2-1), 3xy, (\sqrt{5}/2)(3y^2-1)\right] \tag{39}$$

$$\mathbf{f}_x^T = \left[1, \sqrt{3}x\right], \qquad \mathbf{f}_y^T = \left[1, \sqrt{3}y\right]$$

Dual: $$\mathbf{f}_+^T = \left[1, \sqrt{3}x, \sqrt{3}y\right] \tag{40}$$

$$\mathbf{f}_x^T = \mathbf{f}_y^T = \left[1, \sqrt{3}x, \sqrt{3}y, (\sqrt{5}/2)(3x^2-1), 3xy, (\sqrt{5}/2)(3y^2-1)\right]$$

When these trial functions are substituted into the forgoing expressions both modified primal and dual methods yield results that are identical to those obtained analytically from the second-order primal method. Thus both modified methods are candidates for use in treating voids using higher-order spherical harmonics expansions. Here the modified primal approach is chosen and presented in the following section. An apparent drawback to the corresponding dual approach is briefly discussed in section 6.

5. Transport Formulation

Beginning with the within-group transport equation with isotropic scattering

$$\hat{\Omega}\cdot\vec{\nabla}\psi(\vec{r},\hat{\Omega}) + \sigma\psi(\vec{r},\hat{\Omega}) = \sigma_s\phi(\vec{r}) + s(\vec{r}), \tag{41}$$

we may divide the angular flux into even and odd angular parity components

$$\psi^{\pm} = \tfrac{1}{2}\left[\psi(\vec{r},\hat{\Omega}) \pm \psi(\vec{r},-\hat{\Omega})\right]. \tag{42}$$

The even- and odd- parity components of Eq. (41) are then the coupled equations:

$$\hat{\Omega}\cdot\vec{\nabla}\psi^- + \sigma\psi^+ = \sigma_s\phi + s, \tag{43}$$

and

$$\hat{\Omega}\cdot\vec{\nabla}\psi^+ + \sigma\psi^- = 0, \tag{44}$$

which reduce to Eqs. (1) and (2) when the diffusion approximation is applied. We obtain the weak form by multiplying Eq. (43) by an even-parity weight function, $\tilde{\psi}^+$, and integrating over space and angle:

$$\int dV \int d\Omega \tilde{\psi}^+ \left(\hat{\Omega}\cdot\vec{\nabla}\psi^- + \sigma\psi^+ - \sigma_s\phi - s\right) = 0. \tag{45}$$

Applying the divergence theorem then yields

$$\int dV \int d\Omega \left[-(\hat{\Omega}\cdot\vec{\nabla}\tilde{\psi}^+)\psi^- + \sigma\tilde{\psi}^+\psi^+ - \tilde{\phi}(\sigma_s\phi + s)\right] + \int d\Gamma \int d\Omega \hat{\Omega}\cdot\hat{n}\tilde{\psi}^+\psi^- = 0. \tag{46}$$

We next assume that the incoming angular flux that is known on the boundary; we may thus write

$$\psi^+(\vec{r},\hat{\Omega})+\psi^-(\vec{r},\hat{\Omega})-\psi_\Gamma(\vec{r},\hat{\Omega})=0, \qquad \vec{r}\in\Gamma,\ \hat{n}\cdot\hat{\Omega}<0 \quad (47)$$

where we use the subscript to denote that ψ_Γ is known on the boundary Γ. Modified natural conditions are specified by first forming weighted residuals

$$2\int d\Gamma \int_{\hat{n}\cdot\hat{\Omega}<0} d\Omega\ \hat{\Omega}\cdot\hat{n}\tilde{\psi}^+(\psi^+ +\psi^- -\psi_\Gamma)=0. \quad (48)$$

Using angular parity arguments, we may rewrite this expression as

$$\int d\Gamma \int d\Omega\ \hat{\Omega}\cdot\hat{n}\tilde{\psi}^+\psi^- = \int d\Gamma \int d\Omega \left|\hat{\Omega}\cdot\hat{n}\right|\tilde{\psi}^+\psi^+ +2\int d\Gamma \int_{\hat{n}\cdot\hat{\Omega}<0} d\Omega\ \hat{\Omega}\cdot\hat{n}\tilde{\psi}^+\psi_\Gamma. \quad (49)$$

Combining Eqs. (46) and (49), we then have

$$\begin{aligned}&\int dV \int d\Omega\left[-(\hat{\Omega}\cdot\vec{\nabla}\tilde{\psi}^+)\psi^- +\sigma\tilde{\psi}^+\psi^+ -\tilde{\phi}(\sigma_s\phi+s)\right]\\ &\quad+\int d\Gamma \int d\Omega \left|\hat{\Omega}\cdot\hat{n}\right|\tilde{\psi}^+\psi^+ +2\int d\Gamma \int_{\hat{n}\cdot\hat{\Omega}<0} d\Omega\ \hat{\Omega}\cdot\hat{n}\tilde{\psi}^+\psi_\Gamma=0\end{aligned} \quad (50)$$

Finally, the weak form of Eq. (44) is obtained by weighting by the odd-parity function $\tilde{\psi}^-$ and integrating over space and angle:

$$\int dV \int d\Omega\tilde{\psi}^-\left(\hat{\Omega}\cdot\vec{\nabla}\psi^+ +\sigma\psi^-\right)=0. \quad (51)$$

Suppose that from Eqs. (50) and (51) we can solve for ψ^+ and ψ^-, given s and ψ_Γ for the incoming angles. Analogous to Eq. (48), we can construct the outgoing flux distribution, ψ_Γ, from

$$2\int d\Gamma \int_{\hat{n}\cdot\hat{\Omega}>0} d\Omega\ \hat{\Omega}\cdot\hat{n}\tilde{\psi}^+(\psi^+ +\psi^- -\psi_\Gamma)=0, \quad (52)$$

or equivalently

$$\int d\Gamma \int d\Omega \left|\hat{\Omega}\cdot\hat{n}\right|\tilde{\psi}^+\psi^+ +\int d\Gamma \int d\Omega\ \hat{\Omega}\cdot\hat{n}\tilde{\psi}^+\psi^- -2\int d\Gamma \int_{\hat{n}\cdot\hat{\Omega}>0} d\Omega\ \hat{\Omega}\cdot\hat{n}\tilde{\psi}^+\psi_\Gamma=0. \quad (53)$$

Note that in the diffusion approximation where $\tilde{\psi}^+(\vec{r},\hat{\Omega})\to\tilde{\phi}(\vec{r})$ & $\psi^+(\vec{r},\hat{\Omega})\to\phi(\vec{r})$, and with $\vec{J}=\int d\Omega\hat{\Omega}\psi^-$, Eq. (48) reduces to

$$\int d\Gamma \tilde{\phi} \left[\tfrac{1}{4}\phi - \tfrac{1}{2}\hat{n}\cdot\vec{J} - \int_{\hat{n}\cdot\hat{\Omega}<0} d\Omega \left|\hat{\Omega}\cdot\hat{n}\right| \psi_\Gamma \right] = 0, \qquad (54)$$

the definition of the incoming partial current, J_n^-. Likewise, for $\tilde{\psi}^+(\vec{r},\hat{\Omega}) \to \tilde{\phi}(\vec{r})$ and, $\psi^+(\vec{r},\hat{\Omega}) \to \phi(\vec{r})$, Eq. (53) reduces to

$$\int d\Gamma \tilde{\phi} \left[\tfrac{1}{4}\phi + \tfrac{1}{2}\hat{n}\cdot\vec{J} - \int_{\hat{n}\cdot\hat{\Omega}>0} d\Omega\, \hat{\Omega}\cdot\hat{n}\, \psi_\Gamma \right] = 0, \qquad (55)$$

which is just the definition of the outgoing partial current J_n^+. Thus the modified primal diffusion formulation given by Eqs. (4), (14) and (16) may be replaced by Eqs. (50), (51) and (53) if higher-order spherical harmonics expansions are needed.

6. Discussion

Based on the forgoing analysis of the diffusion approximation, the modified primal mixed method set fourth in section 5 appears to offer an attractive path toward obtaining response matrices for void regions. Moreover, it seems likely that modified primal method may be implemented by making somewhat minor changes to the coding of Smith, et. al. (2004). That said, it remains true that quite high-order spherical harmonics expansions will be required to obtain reasonable accuracy, since neutron distributions in void regions are frequently highly peaked in angle

As an alternative to the modified primal method set fourth in section 5, a modified dual formulation of the transport equation may also be considered. If we were to go through the parallel procedure for the dual formulation, in which the divergence theorem is applied to Eq. (51) instead of Eq. (45), reducing the results to the diffusion approximation would not have yielded partial currents. In the plane geometry, for example, the transport case reduces not to the result given in the previous sections but to continuity of the quantities $\frac{1}{4}\phi \pm \frac{9}{16}J$ rather than the partial currents $J^\pm$ required to conserve neutron balance. Why weak formulation and reduction to diffusion theory are reversible for the modified primal but not the modified dual method deserves further investigation. The difference seems likely to stem from the subtleties of mixed-hybrid continuity requirements studied by Van Criekingen (2004).

Acknowledgements

The author expresses appreciation to M. A. Smith and S. Van Criekingen whose work and discussions contributed greatly to the foundations for this paper

References

Carrico, C. B., Lewis, E. E., and Palmiotti, G., 1992, Three-Dimensional Variational Nodal Transport Methods for Carteian, Triangular and Hexagonal Criticality Calculations, Nucl. Sci. Eng. 111, 168

Carrico, C. B., Lewis, E. E., and Palmiotti, G. , 1994, Matrix Rank in Variational Nodal Approximations, Trans. Am. Nucl. Soc., 70, 162

deOliveira, C. R. C., 1986, An Arbitrary Geometry Finite Element Method for Multigroup Neutron Transport with Anisotropic Scattering, Progress in Nuclear Energy 18, 227

Lewis, E. E. , Carrico, C. B., and Palmiotti, G., 1996, Variational Nodal Formulation of the Spherical Harmonics Equations, Nucl. Sci. Eng. 122, 194

Lewis, E. E. and Palmiotti, G. , 1998, "Red-Black Response Matrix Acceleration by Transformation of Interface Variables," Nucl. Sci. Eng. 130, 1-13

Lindahl, S. and Weiss, Z., 1981, "The Response Matrix Method," Adv. Nucl. Sci. Technol., 13, 72

Smith, M. A., Palmiotti, G., and Lewis, E. E., 2004 , First-Order Spherical Harmonics Formulation Capable of Treating Low Density and Void Regions within the Framework of VARIANT, Proc. PHYSOR_2004 Tpg. Mtg on the Physics of Fuel Cycles and Advanced Nuclear Systems: Global Developments, Chicago, April 2004

Van Criekingen, S., 2004, Mixed-Hybrid Discretization Methods for the Linear Transport Equation, unpublished Ph.D dissertation, Northwestern University

Van Criekingen, S., Lewis, E. E., and Beauwens, R. 2004, Mixed-Hybrid Methods for the Linear Transport Equation, Proc. PHYSOR_2004 Tpg. Mtg on the Physics of Fuel Cycles and Advanced Nuclear Systems: Global Developments, Chicago, April 2004

TABLE 1.
Summary of Weak Form Diffusion Formulations

Primal Equations	
first-order coupled:	Eqs. (5), (4), and (7)
second-order:	Eqs. (6), and (7)
modified first-order coupled	Eqs. (14), (4), and (16)
modified second-order	Eqs. (15), and (16)
Dual Equations	

first-order coupled:	Eqs. (8), (3) and (10)
second-order:	Eqs. (9), and (10)
modified first-order coupled	Eqs. (18), (3), and (20)
modified second-order	Eqs. (19), and (20)